USGS
science for a changing world

Prepared in cooperation with the Bureau of Land Management

Quantifying the Eroded and Deposited Mass of Mercury-Contaminated Sediment by Using Terrestrial Laser Scanning at the Confluence of Humbug Creek and the South Yuba River, Nevada County, California, 2011–13

Scientific Investigations Report 2019–5104

U.S. Department of the Interior
U.S. Geological Survey

Front Cover. Study site at the confluence of the South Yuba River and Humbug Creek. Photograph taken by J.F. Howle, October 3, 2012.

Back cover. Faro laser scanner on standard survey tripod atop bedrock outcrop at South Yuba River–Humbug Creek study site. Photograph taken by J.F. Howle, October 25, 2012.

Quantifying the Eroded and Deposited Mass of Mercury-Contaminated Sediment by Using Terrestrial Laser Scanning at the Confluence of Humbug Creek and the South Yuba River, Nevada County, California, 2011–13

By James F. Howle, Charles N. Alpers, Jeffrey Kitchen, Gerald W. Bawden, and Sandra Bond

Prepared in cooperation with the Bureau of Land Management

Scientific Investigations Report 2019–5104

U.S. Department of the Interior
U.S. Geological Survey

U.S. Department of the Interior
DAVID BERNHARDT, Secretary

U.S. Geological Survey
James F. Reilly II, Director

U.S. Geological Survey, Reston, Virginia: 2019

Suggested citation:
Howle, J.F., Alpers, C.N., Kitchen, J., Bawden, G.W., and Bond, S., 2019, Quantifying the eroded and deposited mass of mercury-contaminated sediment by using terrestrial laser scanning at the confluence of Humbug Creek and the South Yuba River, Nevada County, California, 2011–13: U.S. Geological Survey Scientific Investigations Report 2019–5104, 30 p., https://doi.org/10.3133/sir20195104.

Associated data for this publication:
Howle, J.F., 2019, Terrestrial laser scanning data from the confluence of the South Yuba River and Humbug Creek, Nevada County, California, 2011–2013: U.S. Geological Survey data release, https://doi.org/10.5066/P9EOI74U.

ISSN 2328-0328 (online)

Acknowledgments

Funding for this project was provided to the U.S. Geological Survey by the Bureau of Land Management (BLM) under Interagency Agreement L12PG00295. The authors thank Peter Graves at the BLM for project management.

Contents

Figures

Tables

Conversion Factors

International System of Units to U.S. customary units

Multiply	By	To obtain
	Length	
millimeter (mm)	0.03937	inch (in.)
centimeter (cm)	0.3937	inch (in.)
decimeter (dm)	3.937	inch (in.)
meter (m)	3.281	foot (ft)
kilometer (km)	0.6214	mile (mi)
meter (m)	1.094	yard (yd)
	Area	
square meter (m^2)	0.0002471	acre
square centimeter (cm^2)	0.001076	square foot (ft^2)
square meter (m^2)	10.76	square foot (ft^2)
square centimeter (cm^2)	0.1550	square inch (ft^2)
	Volume	
cubic centimeter (cm^3)	0.06102	cubic inch (in^3)
cubic meter (m^3)	35.31446	cubic foot (ft^3)
	Mass	
gram (g)	0.03527	ounce, avoirdupois (oz)
kilogram (kg)	2.205	pound avoirdupois (lb)
	Density	
gram per cubic centimeter (g/cm^3)	62.4220	pound per cubic foot (lb/ft^3)

Temperature in degrees Celsius (°C) may be converted to degrees Fahrenheit (°F) as

$$°F = (1.8 \times °C) + 32.$$

Temperature in degrees Fahrenheit (°F) may be converted to degrees Celsius (°C) as

$$°C = (°F - 32) / 1.8.$$

Datum

Vertical coordinate information is referenced to the North American Vertical Datum of 1988 (NAVD 88).

Horizontal coordinate information is referenced to the North American Datum of 1983 (NAD 83).

Elevation, as used in this report, refers to distance above the vertical datum.

Supplemental Information

Concentrations of chemical constituents in sediment are given in nanograms per gram (ng/g).

Abbreviations

1-SD	one-standard deviation
2-D	two-dimensional
2-SD	two-standard deviation
3-D	three-dimensional
AEP	annual exceedance probability
AR	atmospheric river
BLM	Bureau of Land Management
CSG	crest-stage gage
DA	drainage area
HWM	high-water mark
KeckCAVES	W.M. Keck Center for Active Visualization in the Earth Sciences (at the University of California, Davis)
Lidar	light detection and ranging (or LiDAR)
NWS	National Weather Service
QA	quality assurance
RMSE	root-mean-square error
TIN	triangulated irregular network
T-lidar	terrestrial lidar
TLS	terrestrial laser scanning
UCD	University of California, Davis
USGS	United States Geological Survey
WY	water year

Note that selected technical terms are defined in the Glossary. These terms are indicated in **bold font** the first time they appear in the main body of the report.

Quantifying the Eroded and Deposited Mass of Mercury-Contaminated Sediment by Using Terrestrial Laser Scanning at the Confluence of Humbug Creek and the South Yuba River, Nevada County, California, 2011–13

By James F. Howle, Charles N. Alpers, Jeffrey Kitchen, Gerald W. Bawden, and Sandra Bond

Abstract

High-resolution, terrestrial laser scanning, also known as ground-based lidar (light detection and ranging), was used to quantify the volume of mercury-contaminated sediment eroded from an outcrop of historical placer-mining debris at the confluence of Humbug Creek and the South Yuba River in the Sierra Nevada foothills, about 17 kilometers northeast of Grass Valley, California, and delivered to a zone below an observed flood stage of the South Yuba River. Substantial quantities of mercury were used and lost to the environment from historical placer gold mining activities on the western slope of the Sierra Nevada, California, and recent studies have documented continued persistence of mercury and methylmercury concentrations in water, sediment, fish, and predatory invertebrates in the Yuba River drainage basin in relation to suspected mercury sources. To identify areas that have high levels of mercury contamination as possible remediation targets in the Yuba River drainage basin and other areas in the Sierra Nevada, the U.S. Geological Survey worked in cooperation with the Bureau of Land Management on this and other detailed studies. Malakoff Diggings, one of the largest hydraulic gold mines in the Sierra Nevada, is 3.5 kilometers north of the study site in the Humbug Creek subbasin.

Terrestrial laser scanning was used to produce centimeter-scale, three-dimensional maps of the complex outcrop surface, which was composed of an upper erosional area (cliff and over-steepened slope) and a lower depositional area (colluvial slope). The outcrop could not be mapped non-destructively or in sufficient detail by traditional surveying techniques. The study site, which was approximately 70 meters long, 30 meters wide and 20 meters high, was surveyed four times in 2 years (December 15, 2011; October 25, 2012; January 4, 2013; and November 22, 2013) to determine volumetric differences in the upper erosional and lower depositional areas between surveys. Measured changes in volume for the upper erosional area and lower depositional area were multiplied by the corresponding sediment density so that a mass-balance relationship, between the eroded and deposited sediment during each period, could be used to estimate the amount of mercury-contaminated sediment that was transported to below the base of the colluvial slope, where it could be mobilized by the South Yuba River during a flood having a 5-to-10-year recurrence interval. On December 2, 2012, a flood of this estimated magnitude reached the base of the colluvial slope.

Between the first and second surveys (December 15, 2011–October 25, 2012), an estimated mass of 18±9.2 kilograms of sediment was transported from steeper slopes to the gently sloping river bank below the base of the colluvial slope. Between the second and third surveys (October 25, 2012–January 4, 2013), an atmospheric river caused heavy precipitation at the study site during late November and early December 2012. This short-duration, high-intensity rain resulted in a large amount of erosion and deposition at the study site and also caused high streamflow (flood stage) in the South Yuba River. From October 2012 to January 2013, 51±31 kilograms of sediment was transported to below the base of the colluvial slope, that is, below the high-water mark of December 2, 2012. Between the third and fourth surveys (January 4, 2013–November 22, 2013), an additional 10±26 kilograms of sediment was transported to below the base of the colluvial slope. During the 24 months of the study, the total mass of sediment delivered below the base of the colluvial slope and the high-water mark of December 2, 2012, was 79±66 kilograms.

In any given year there is a 10–20-percent chance (5-to-10-year recurrence interval) of a flood equal to or greater than that of the December 2, 2012, flood, which could transport mercury-contaminated sediment at the study site into the South Yuba River. Hydraulically modeled estimates of the South Yuba River stage during floods having a 50- and 100-year recurrence interval (2- and 1-percent annual exceedance probability, respectively) indicated that resulting river stages could be 2.2–3.0 meters above the base of the colluvial slope, or 2.2–3.0 meters above the high-water mark of December 2, 2012. Such high river stages would be likely to inundate the lower half of the colluvial slope and mobilize a substantial volume of mercury-contaminated sediment to downstream areas.

Introduction

Historical **hardrock** (lode) and **placer** (gravel) gold mines on the western slope of the Sierra Nevada, California, produced substantial volumes of mercury-contaminated **mining debris** (Gilbert, 1917; James, 1989; Nakamura and others, 2018). During the mid-to-late 1800s and the early 1900s, elemental mercury was used extensively to increase gold recovery (Alpers and others, 2005a), which resulted in mercury contamination of sediment in many areas of the Sierra Nevada, including the South Yuba River drainage basin and the Humbug Creek subbasin (fig. 1). Historical records indicate that substantially more mercury was used and lost to the environment from placer gold mining activities in the Sierra Nevada than from hardrock mines and associated mills (Churchill, 2000; Alpers and others, 2005a). Accumulation of mercury-contaminated sediment downstream from historical gold-mining sites in the South Yuba River has been documented at Englebright Lake (Alpers and others, 2006), behind Daguerre Point Dam (Hunerlach and others, 2004), and as far downstream as San Francisco Bay (Hornberger and others, 1999).

To identify areas that have high levels of mercury contamination as possible remediation targets in the Yuba River drainage basin and other areas in the Sierra Nevada, the U.S. Geological Survey (USGS) has been working in cooperation with the Bureau of Land Management (BLM) and other federal, state, and local agencies on regional and detailed studies since 1999 (Hunerlach and others, 1999, 2004; May and others, 2000; Alpers and others, 2005a, 2005b, 2006, 2012; Fleck and others, 2011; Marvin-DiPasquale and others, 2011; Alpers and others, U.S. Geological Survey, written commun., June 2013). These efforts have resulted in remediation of several abandoned mine sites (Alpers, 2017). In the Yuba River drainage basin, methylmercury concentrations in water, sediment, fish (primarily Brown Trout and Largemouth Bass), and predatory invertebrates (larval or immature caddisflies, dobsonflies, dragonflies, and stoneflies, and adult water striders) were monitored at selected locations (2010–12) to assess the temporal and spatial variability upstream and downstream from suspected mercury sources, including the study site (Alpers and others, U.S. Geological Survey, written commun., June 2013; Fleck and others, U.S. Geological Survey, written commun., June 2013; Alpers and others, 2016; Stumpner and others, 2018).

The study site is at the confluence of Humbug Creek and the South Yuba River, approximately 17 kilometers (km) northeast of Grass Valley, California (fig. 1). Malakoff Diggings, one of the largest **hydraulic gold mines** in the Sierra Nevada, is 3.5 km north of the study site in the Humbug Creek subbasin. In addition, there are other smaller hydraulic gold mines (Le Du and Old Glory) upstream from the study site near North Bloomfield, California (formerly Humbug City, fig. 1*B*). During the 1870s, the lower reaches of the Humbug Creek drainage (fig. 2*A*) were filled with mercury-contaminated sediment (mining debris) from upstream hydraulic gold mines. The sediment was transported to the South Yuba River canyon, forming an alluvial fan that temporarily dammed the river to the top of the cliff, approximately 24 meters (m) above the modern base-flow stage (fig. 2*B*). The South Yuba River subsequently cut through the alluvial dam and created a steep, approximately 21-m-high outcrop of mercury-contaminated sediment parallel to the river. The average mercury concentration was 1,200 nanograms per gram (ng/g, or parts per billion) in two composite sediment samples collected during September 2008 from the outcrop and sieved to the silt-and-clay fraction, less than 0.063 millimeter (mm; Fleck and others, 2011). Ten additional sediment samples from the same outcrop that were sampled in 2012 and also sieved to less than 0.063 mm had an average mercury concentration of 2,520 ng/g and a standard deviation of 704 ng/g (Marvin-DiPasquale and Agee, U.S. Geological Survey, written commun., 2013). Coarser size fractions from the outcrop had lower mercury concentrations (Fleck and others, 2011): the size fraction between 0.063 and 0.25 mm was 143±23 ng/g (n=5), and the fraction between 0.25 and 1.0 mm had 62±5 ng/g (n=3). Exposed sediment in the steep part of the outcrop (cliff and over-steepened slope) has been eroding and deposited on the unconsolidated **colluvial slope** below it (fig. 2*B*). During high streamflow, the South Yuba River can mobilize unconsolidated sediment from the colluvial slope, increasing the potential for mobilization of mercury to downstream areas.

Terrestrial laser scanning (TLS) is a remote-sensing technology that can collect high-resolution (sub-centimeter), three-dimensional (3-D) measurements of the land surface that cannot be achieved with traditional surveying techniques (Heritage and Large, 2009). A laser scanner emits pulses of near-infrared laser light that are timed to measure the distance (range) from the laser scanner to the reflecting surface. Laser ranges are combined with angular orientation data to generate a dense and detailed set of points (x, y, and z coordinates of individual laser returns), referred to as a **point cloud**. The non-destructive measuring of the cliff, over-steepened slope, and colluvial slope surfaces on multiple occasions and the sub-centimeter resolution of the point cloud allow for a spatially detailed assessment of topographic change and a quantitative measurement of the volume of erosion (or deposition) between scan-collection dates.

Four sequential TLS surveys of the study site were completed during a 24-month period. Each survey was composed of six TLS scans from different vantages that were combined in a composite 3-D point cloud of the study site. The surveys were co-registered, or ‘aligned,’ in a common reference frame so that volumetric comparisons between the surveys could be made. The volumetric differences between surveys quantified the volume of sediment eroded from the cliff and over-steepened slope and also the volume of sediment deposited on the colluvial slope below. The measured volumes of eroded and deposited sediment were converted to mass and differenced to estimate the amount of sediment transported to below the base of the colluvial slope, coinciding with a high-water stage of the South Yuba River documented during the study.

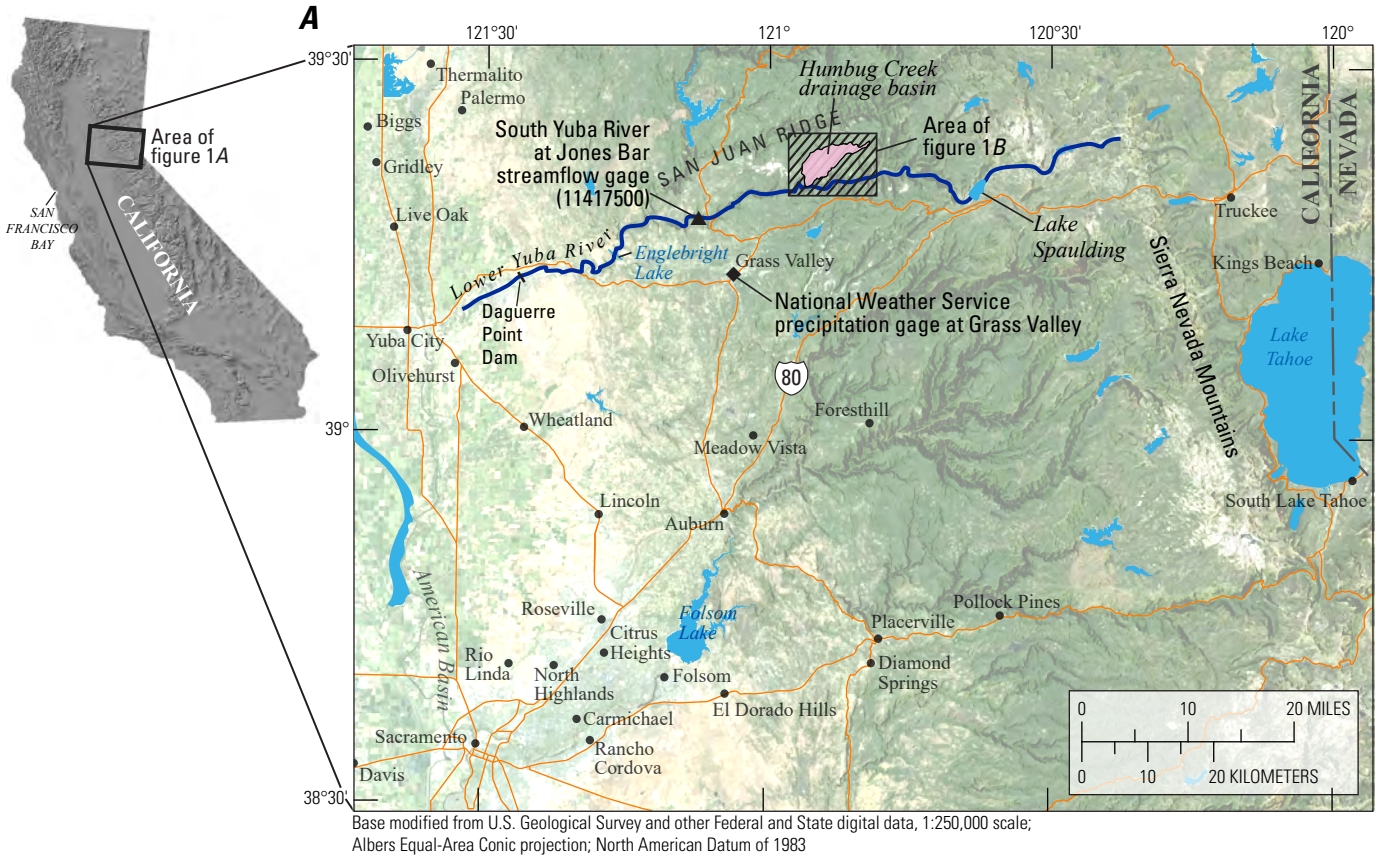

Figure 1. Areas discussed in the text: *A*, the Humbug Creek drainage basin and the South Yuba River, northern California; *B*, detailed map of the Humbug Creek drainage basin, Malakoff Diggings mine pit, and Humbug Creek–South Yuba River study site.

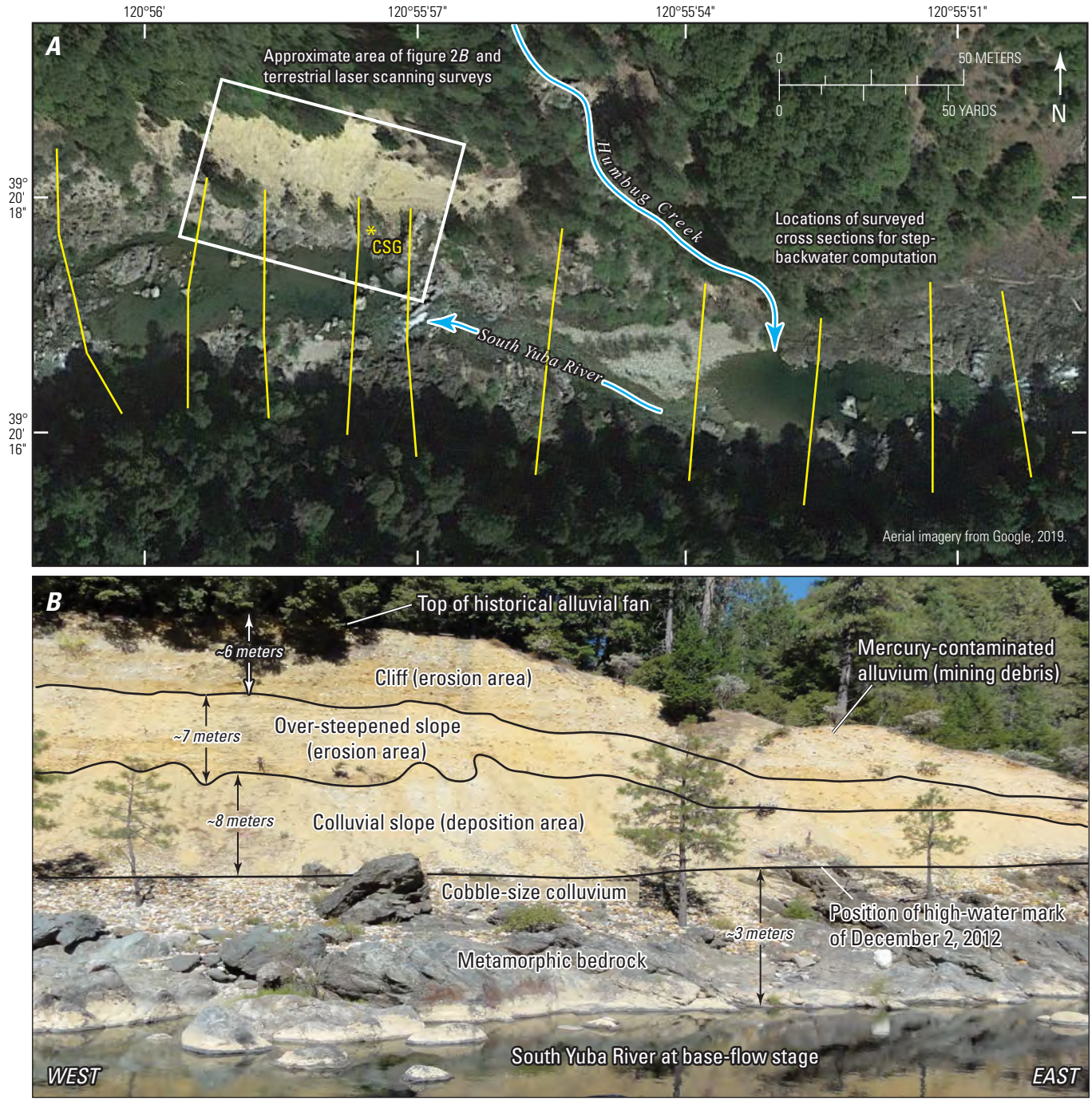

Figure 2. Study site at the confluence of the South Yuba River and Humbug Creek: *A*, aerial view of the approximate area of terrestrial laser scanning surveys, locations of surveyed cross sections, the crest-stage gage (CSG), and direction of streamflow; *B*, study site looking north showing cliff area, over-steepened slope area, colluvial slope, and position of high-water mark of the South Yuba River from December 2, 2012. Photograph taken October 3, 2012.

Purpose and Scope

The purpose of this report is to document the methods used to quantify the volume of mercury-contaminated sediment eroded and deposited on different parts of an outcrop of hydraulic mining debris near the Humbug Creek–South Yuba River confluence; estimate the amount (mass) of sediment delivered from the outcrop to the zone below an observed flood stage (December 2, 2012) for three periods between December 15, 2011, and November 22, 2013; present estimates of annual exceedance probabilities of floods (flood frequencies) for the South Yuba River that are equal to or greater than the flood of December 2, 2012; and provide estimates of how much mercury-contaminated sediment on the colluvial slope could be inundated and potentially mobilized by floods having 1- and 2-percent annual exceedance probabilities (100- and 50-year recurrence floods, respectively).

The results of this study are to be combined with laboratory determinations of mercury concentration and grain-size distribution to quantify the amount of mercury eroded into the South Yuba River downstream from the Humbug Creek confluence. Results from these investigations are to be used by the BLM to determine whether removal or stabilization of mercury-contaminated sediment is needed at the study site.

Study Site Description

The study site is at the confluence of Humbug Creek and the South Yuba River on the western slope of the Sierra Nevada (fig. 1), where the topographic relief is approximately 400 m (approximately 1,300 feet; ft) from the bottom of the South Yuba River canyon to surrounding ridge lines. The study site, at the bottom of the South Yuba River canyon, is at an elevation of approximately 650 m (2,130 ft). The cliff, over-steepened slope, and colluvial slope (fig. 2*B*) are composed of fluvially transported mining debris (alluvium) from upstream, historical hydraulic gold mines (fig. 1). The Humbug Creek subbasin, a major tributary in the South Yuba River drainage basin (fig. 1*A*), ranges in elevation from approximately 650 m at the confluence with the South Yuba River to approximately 1,500 m (4,920 ft) at the headwaters.

The climate in the study area is Mediterranean, with warm-to-hot, dry summers and cool, rainy winters. The nearest and longest precipitation record is from a National Weather Service (NWS) station approximately 17 km to the southwest, at Grass Valley, California (fig. 1). Daily precipitation data for this station for water years (WY) 1967 through 2013 are available at http://www.ncdc.noaa.gov/cdo-web/search; (NWS Station GHCND: USC00043573, GRASS VALLEY NUMBER 2, CA US, last accessed June 11, 2019). The average annual water-year precipitation at Grass Valley, California, was 1.34 m (52.80 inches; in.) for 1967 through 2013. For WY 2011 (October 2010 through September 2011), the total precipitation (1.85 m or 72.81 in.) was 138 percent of the long-term average, whereas the WY 2012 total (1.19 m or 46.74 in.) was 88 percent of the long-term average. In WY 2013, the total precipitation (1.20 m or 47.21 in.) was 89 percent of the long-term average, similar to that of WY 2012.

The closest streamflow gaging station on the South Yuba River is at Jones Bar, approximately 16 km west-southwest (downstream) of the study site (fig. 1). Streamflow discharge data from this stream gage (http://cdec.water.ca.gov/dynamicapp/QueryF?s=JBR) were adjusted to account for the difference in contributing drainage area between the gage and the study site to estimate the streamflow discharge at the study site.

The cliff, over-steepened slope, and colluvial slope areas at the Humbug Creek study site are approximately 70 m long, 30 m wide and have a combined maximum height of about 21 m (fig. 2*B*), covering an approximate area of 2,100 square meters (m^2). The 'erosion area' as defined here is approximately 13 m high (maximum) and is composed of an upper, near-vertical cliff section (fall face) and a lower, over-steepened slope (figs. 2*B*, 3). The upper, near-vertical cliff section (2–6 m in height), exposes poorly sorted, but moderately well-indurated (consolidated or cemented as a result of weathering processes through time) sediments ranging in grain size from large cobble to fine silt and clay. The over-steepened slope (1–7 m in height) is also composed of poorly sorted sediments ranging in grain size from large cobble to fine silt and clay. In contrast to the cliff, these sediments are weakly indurated, forming a steep slope (fig. 3). Because of the steepness of this slope, 38–44 degrees (°), only finer grained particles (sand-size or less) eroding from the upper, near-vertical part of the cliff area come to rest temporarily on the mid-slope. Particles larger than sand size (gravel, 2–64 mm; cobbles, 64–256 mm; and boulders, greater than 256 mm in diameter; Wentworth, 1922) tend to bounce and roll downslope, eventually coming to rest on the colluvial slope (figs. 2*B*, 3). Erosion mechanisms across the near-vertical cliff and the over-steepened slope included persistent gravity-driven **dry-ravel**, collision dislodgement of other particles, raindrop impact, sheet wash, frost heave, and localized mass wasting (block fall). When clumps of the moderately to weakly indurated sediment of the cliff and over-steepened slope erode and fall, bounce, and roll downslope, the sediment disaggregates and becomes less dense as it expands in volume. Consequently, for a given volume of eroded sediment the corresponding volume of sediment deposited on the colluvial slope would be greater because of the change in density.

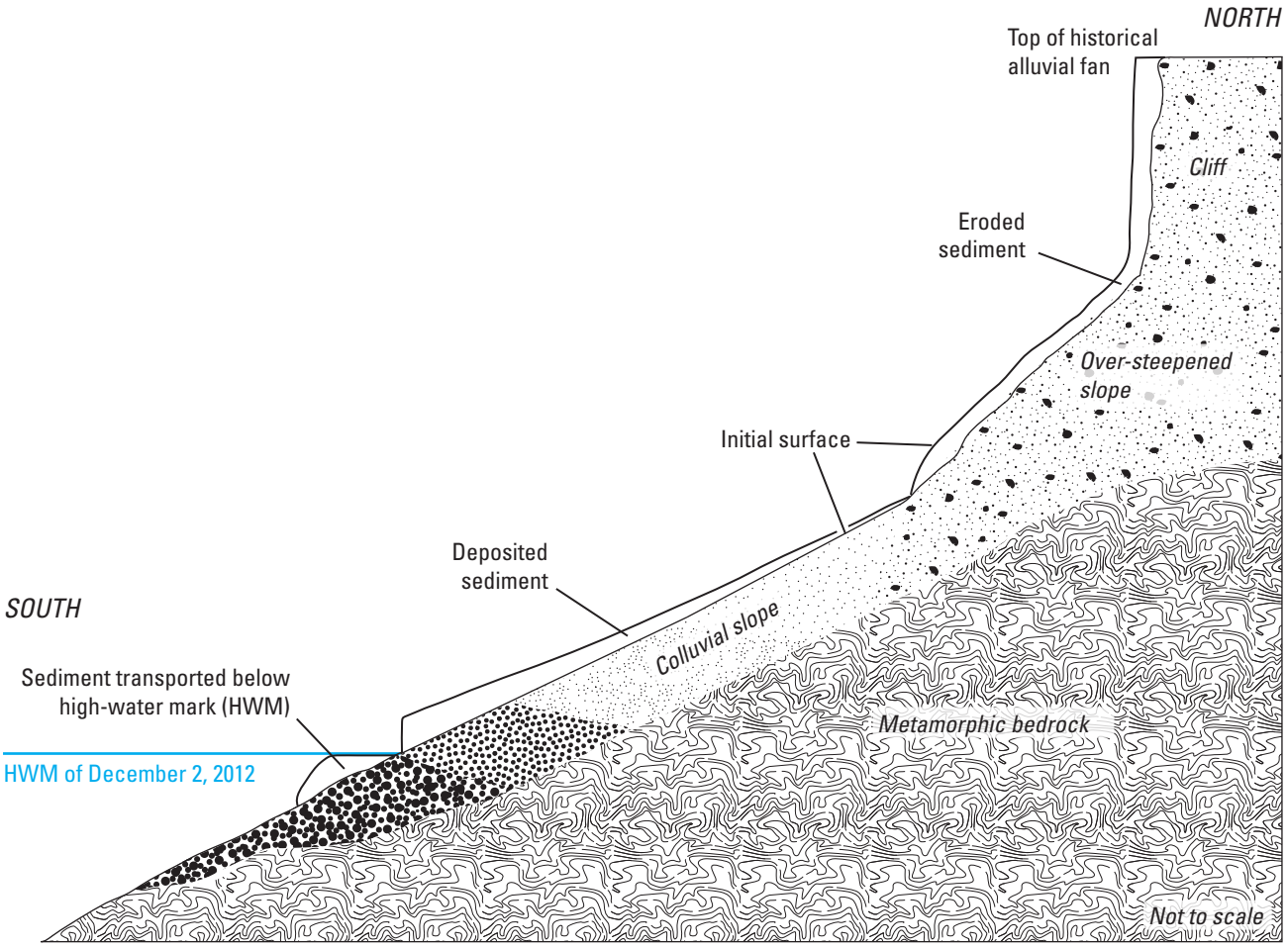

Figure 3. Relative positions of the cliff, over-steepened slope, and colluvial slope at the South Yuba River–Humbug Creek study site and the initial surface, eroded sediment, deposited sediment, and sediment transported below the high-water mark of December 2, 2012.

The colluvial slope (foot slope) was approximately 3–9 m in height and ranged in dip from 34° at the top of the slope to 31° at the base of the slope (figs. 2*B*, 3). Particles eroded from the near-vertical cliff and over-steepened slope and deposited on the lower colluvial slope were fairly well sorted, with finer grain sizes at the top and coarser material at the bottom. The sorting is a function of the momentum generated while particles fall, bounce, and roll downslope. The mass of increasingly larger particles—that is, silt (0.004–0.063 mm), sand (0.063–2 mm), gravel (2–64 mm), cobbles (64–256 mm), and boulders (greater than 256 mm)—generates proportionally more inertia or momentum, which carries the particle farther downslope, depending on particle size and mass. Secondary transport mechanisms of sediment particles on the colluvial slope include gravity-driven rolling, sliding and creep, sheet wash, frost heave, and water-saturated flow (**debris flow**).

Methods

This section contains information on methods of TLS data collection, point-cloud alignment, quality assurance of alignments, and volumetric calculations. Also included is a description of sediment-density measurements.

Terrestrial Laser Scanning Data Collection

Terrestrial laser scanning data were collected on December 15, 2011, October 25, 2012, January 4, 2013, and November 22, 2013, using a FARO Focus^{3D} laser scanner (model S-120, FARO Technologies, Lake Mary, Florida). Laser returns from the FARO scanner have a positional accuracy of plus or minus (±) 0.5 mm at a distance of 25 m (per manufacturer specifications), which was achieved by averaging the return of six laser pulses to determine the x, y, and z coordinates of each recorded point. Points greater than 30 m from the scanner origin were not used in this study. The FARO scanner, mounted on a standard survey tripod, rotated about the vertical axis, collecting a full 360° point cloud, except for a 60º-wide cone directly beneath the scanner. The cliff, over-steepened slope, and colluvial slope areas were scanned from six different vantages along the base of the 70-m-long study site (fig. 4). A pre-set laser spot spacing of 6.7 mm, at a distance 10 m from the scanner origin, was used for all scans. Across the top of the cliff (farthest from the scanner origin), the average data density from the six combined scans was more than 6,400 points per square meter, which was equivalent to a laser-spot spacing of approximately 12 mm. Along the base of the colluvial slope (nearest to the scanner origin), the average data density from the six combined scans was more than 200,000 points per square meter, which was equivalent to a laser spot spacing of less than 0.5 mm.

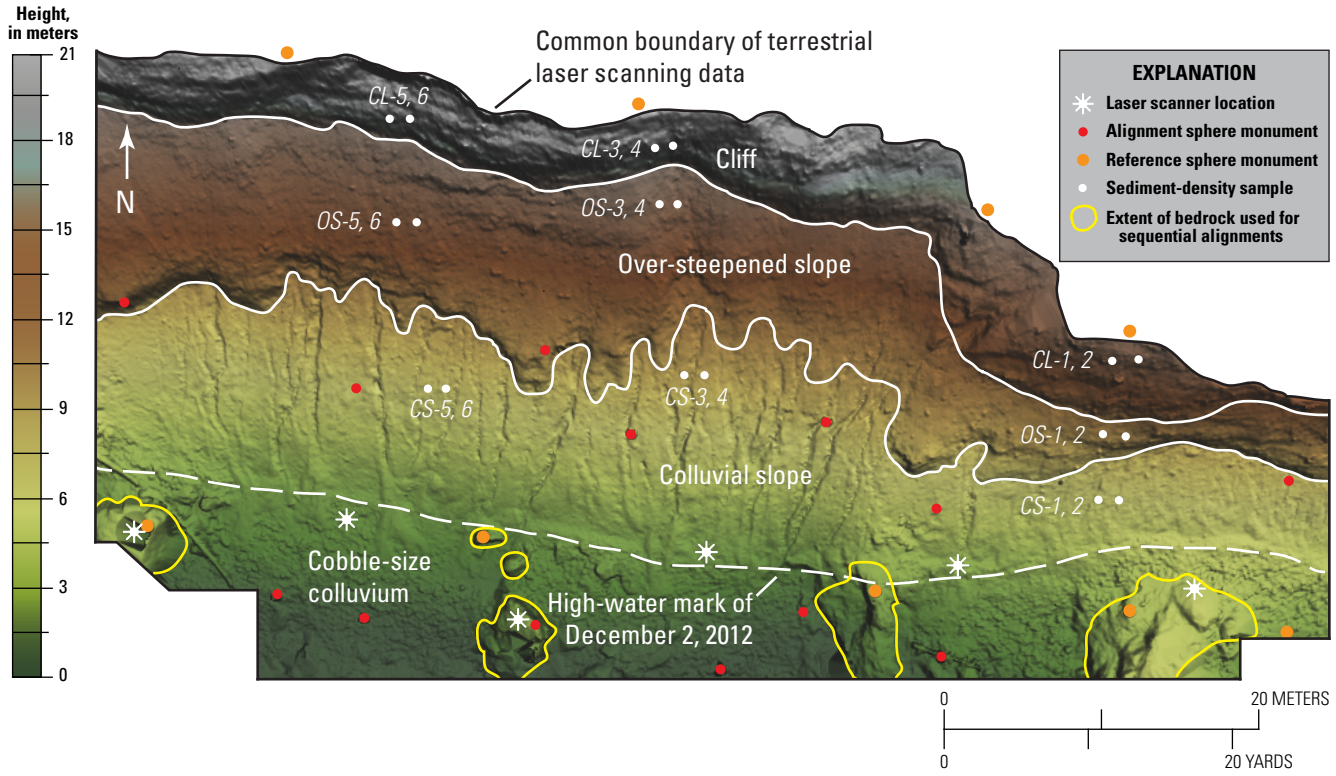

Figure 4. Shaded-relief plan-view image of the South Yuba River–Humbug Creek study site on January 4, 2013, showing the cliff, over-steepened slope, and colluvial slope areas; locations of the laser scanner, alignment and reference sphere monuments, and bedrock outcrops used for sequential alignments; sediment-density sample locations with identifiers (see appendix table 1–1); and the high-water mark (HWM) of the South Yuba River on December 2, 2012, with artificial illumination from the northeast. The image was created by Quick Terrain Modeler™ software (QT Modeler, version 7.0.2, Applied Imagery, Silver Spring, Maryland).

Point-Cloud Alignment

Described in this section is the construction of various types of monuments used to mount alignment and reference spheres. Also discussed are the methods used to align or combine adjacent scans in a given survey, the alignment of sequential surveys, and the quantitative assessment of the quality of alignments.

Alignment Spheres

To align individual scans collected during the same survey (that is, to combine the scans in a common x, y, and z reference frame), the FARO system utilizes spheres of various diameters (0.1, 0.2, and 0.45 m) placed throughout the scan area (figs. 4, 5). Neighboring scans typically had five to six spheres common to both scans that were used for alignment. Some alignment spheres were positioned temporarily on tripods, whereas other spheres were attached magnetically to permanent monuments (fig. 5). The permanent monuments were set by several methods. Along the base of the colluvial slope, where bedrock outcrops were available (figs. 2*B*, 4), holes were drilled into the rock, and the magnetic sphere mounts were anchored with expanding mortar (fig. 5*B*). Trees ranging in diameter from 0.3 to 0.9 m at the base of the colluvial slope and on both sides of the study area were used to mount the spheres by screwing magnetic mounts into the tree trunks (fig. 5). Additionally, three other monuments were established across the colluvial slope (figs. 4, 5) by driving 1.2-m-long, 16-mm-diameter sections of threaded steel rod into the alluvium until 0.1 m of rod was left exposed above the ground surface. The annular spaces around the rods were filled with expanding mortar to anchor the rods in place. Removable 0.45-m-diameter spheres were screwed onto the exposed threaded rods prior to scanning.

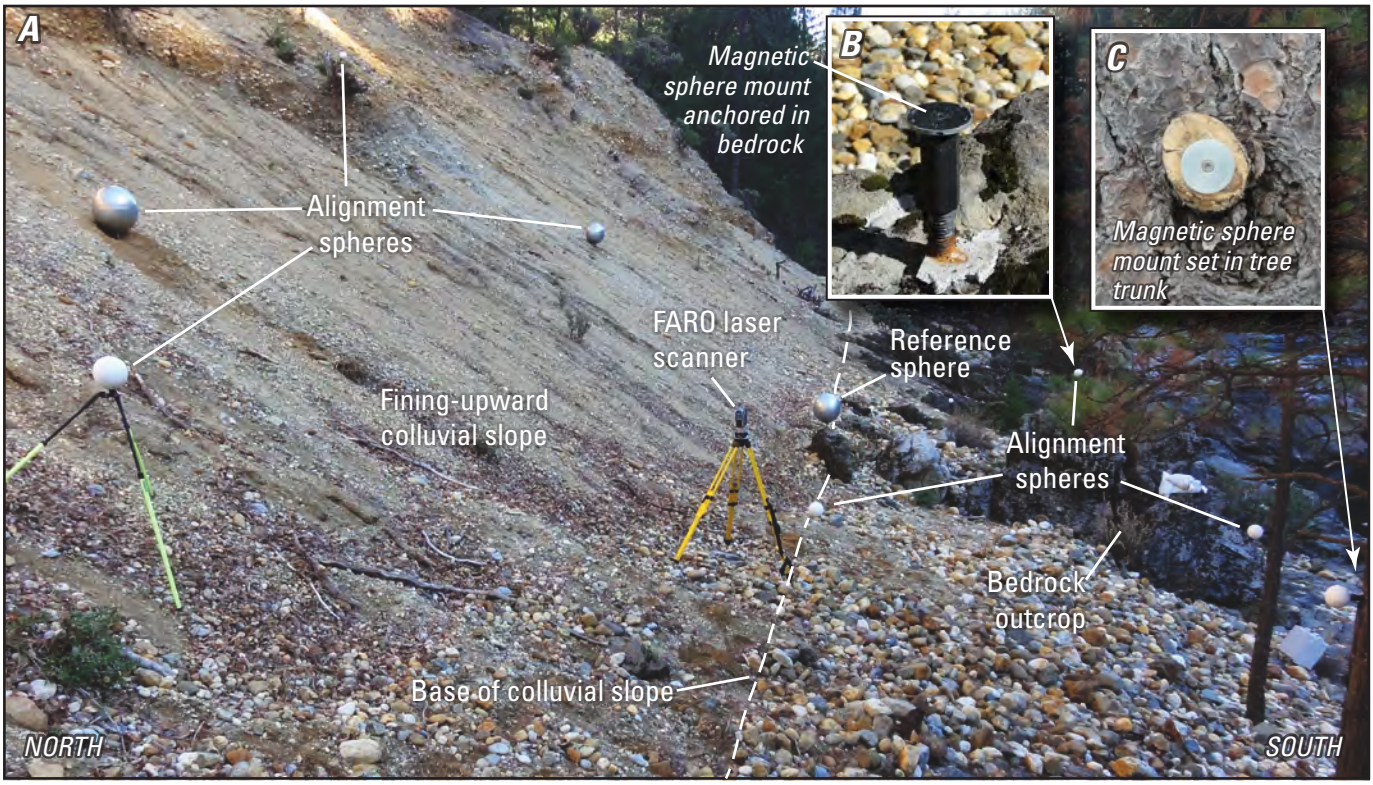

Figure 5. Colluvial slope at the South Yuba River–Humbug Creek study site and monuments used for terrestrial laser scanning data collection: *A*, tripod-mounted FARO laser scanner at the base of the colluvial slope, alignment, and reference spheres; *B*, close up of magnetic sphere mount anchored in bedrock; and *C*, close up of magnetic sphere mount set in a tree trunk.

Reference Spheres

The alignment quality of sequential TLS surveys was assessed quantitatively by using an independent set of reference spheres. At five locations along the base of the study site (fig. 4), 15-centimeter (cm)-deep holes were drilled into the bedrock outcrops, and sections of threaded steel rod (25 cm long and 16 mm in diameter) were anchored in the rock with expanding mortar. Prior to scanning, 0.45-m-diameter reference spheres (dedicated to specific monuments) were screwed onto the stable monuments until the spheres were against the threaded rod. Linear reference marks on the spheres and rod were aligned so that each sphere could be repositioned on the corresponding monument to within 3 mm. Four additional locations across the top of the cliff were used to mount 0.2-m-diameter spheres by screwing magnetic mounts into tree trunks that ranged in diameter from 0.3 to 0.9 m (figs. 4, 5).

Alignment of Scans

The alignment of the six scans in each survey was accomplished using the software package SCENE (version 4.0, FARO Technologies, Lake Mary, Florida). For each scan, the SCENE software automatically identified the alignment spheres (fig. 5) and determined their relative positions. The SCENE software then locked the position of the scan that had the greatest number of alignment spheres, while the remaining scans were rotated and translated until the spheres were best fit in 3-D space as closely as possible relative to the locked scan.

For the purpose of assessing the quality of the alignment, the SCENE software also calculated a 1-standard-deviation (1-SD) error or root-mean-square error (RMSE) of the alignment. This error was computed from the spatial variations of the alignment sphere center points for each unlocked scan relative to the locked scan. The doubled RMSE of the scan alignments was ±3.6 mm for the baseline survey, ±2.5 mm for the second survey, ±1.7 mm for the third survey, and ±2.3 mm for the fourth survey.

Alignment of Surveys

To use the four sequential surveys to calculate volumes of erosion and deposition, stable features common to each survey were needed so that the surveys could be aligned, or co-registered, to the same x-, y-, and z-coordinate system. This study utilized six bedrock outcrops that were exposed along the length of the study site to co-register the sequential surveys (fig. 4). The outcrops of metamorphic bedrock ranged in area from 3 to 40 m^2 and were within 10 m of the laser-scanning locations (figs. 4, 5*A*). This proximity yielded a data density of more than 100,000 points per square meter across the bedrock surfaces, which was equivalent to a laser spot spacing of less than 0.5 mm. The well-defined surface geometry of the irregularly shaped outcrops allowed for a statistically significant matching of the bedrock surfaces between surveys.

The PolyWorks® software package (version 12.0.15, InnovMetric Software Inc., Québec City, Québec, Canada) was used to align the second, third, and fourth surveys (repeat surveys) to the first (baseline) survey. The initial alignment of a repeat survey was done manually. The baseline and repeat surveys were viewed from the same perspective (typically plan view) on dual computer monitors. Pairs of common features (such as distinct points on rocks and tree trunks) in each survey were identified, and the software then translated the repeat survey to the coordinate system of the baseline survey. The initial placement typically produced alignments within 6–8 cm.

The next step in the alignment process was isolating the bedrock surfaces in the baseline survey to be matched to the subsequent surveys. In a 3-D visualization environment, the points of the bedrock outcrops were isolated and identified as alignment points. Only those points representing the 3-D extent of the bedrock outcrops were used for the fine-scale alignment. The centimeter-scale misalignment (from the initial manual placement) was automatically corrected with an iterative algorithm that computed an optimal alignment by minimizing the distance between the 3-D point clouds of the bedrock surfaces in the baseline and those in subsequent surveys. Through a series of rotations and translations, the repeat surveys were adjusted until a user-defined convergence (for this study, 0.1 mm or less) between the baseline and subsequent surveys was achieved.

Survey-Alignment Error

After a repeat survey was aligned to the baseline survey, a quantitative assessment of the alignment was done using the nine reference spheres shown in fig. 4. These reference spheres, independent from the alignment spheres, were only used for quality-assurance (QA) purposes. Reference-sphere center points were defined from the point clouds by using the PolyWorks® software package. The spherical point clouds (more than 10,900 points per sphere on average) were isolated and modeled as perfect spheres of a known radius. From these best-fit spheres, the center points were derived mathematically as unique (x, y, and z) points in 3-D space at sub-millimeter resolution. The repeatability of defining these points for any given sphere was ±0.4 mm (maximum variance along x, y, or z axis).

For the nine reference spheres in the baseline and subsequent surveys, the corresponding x, y, and z center-point coordinates were tabulated and differenced. For each center point, the variance along each axis was used to calculate the RMSE of the alignment. The alignment of the second survey (October 2012) relative to the baseline survey (December 2011) had an RMSE of 4.5 mm. For the third survey (January 2013), the RMSE relative to the baseline survey was 4.6 mm; for the fourth survey (November 2013), the RMSE was 6.0 mm. The quantitative center-point RMSE assessment of the alignments (1-SD error) was about 4.5–6.0 mm, which provided a doubled RMSE interval, ranging from 9.0 to 12.0 mm, for these alignments. Precise 3-D measurements, discussed in the next section, comparing the stable reference spheres in each survey, confirmed the doubled RMSE interval of about 9–12-mm uncertainty for the alignment of sequential surveys.

Quality Assurance of Alignments

This study used the University of California, Davis (UCD), W.M. Keck Center for Active Visualization in the Earth Sciences (KeckCAVES) and the Virtual Reality User Interface "LiDAR Viewer" software (Kreylos and others, 2008) to visually inspect the **lidar** point-cloud data for QA of the alignment of overlapping scans in a single period, as well as the alignments of sequential surveys. Immersion in lidar point-cloud data by using 3-D virtual-reality technologies offers a unique and powerful tool to visualize complex 3-D data sets that cannot be seen on a conventional, two-dimensional (2-D) computer screen. At the UCD KeckCAVES, lidar point-cloud data were projected stereoscopically (with four projectors) onto the floor, back wall, and side walls of a 3-m-square room (or "cave"). Motion-capture glasses that move the scenery in accordance with head movements were used in the cave to create a fully immersive visualization environment. Using a hand-held controller, the user was able to move through the 3-D data, enlarging it to a scale greater than 1:1, as needed. Full immersion with the 3-D data enabled the inspection and isolation of features more intuitively, quickly, and accurately than previously possible with non-immersive 2-D environments, such as desktop computers (Kellogg and others, 2008; Kreylos and others, 2008).

To verify the alignment of overlapping scans for a single period, the data from each scan were color-coded so that one scan could be easily differentiated from another. Within the area of overlap, features such as planar bedrock surfaces, distinctly shaped cobbles, and reference spheres were isolated at a scale greater than or equal to 1:1. By selecting common points with the hand-held controller, precise distances between overlapping scans were measured. These measurements were compared with the previously discussed statistical uncertainties generated by the SCENE alignment software to verify those values. Similarly, for the alignments of sequential surveys, each survey was color-coded and distances between distinct points on the bedrock surfaces were measured; the measured differences were then compared to the previously discussed RMSE to confirm those values.

Volumetric Determination

Before differences in volume could be calculated, additional steps were needed to remove unwanted points, to create surfaces from the land-surface points, to define a common perimeter, and to isolate the areas of erosion (cliff and over-steepened slope areas) and deposition (colluvial slope area) within the common perimeter.

Data-Point Removal

Areas of vegetation scattered across the surface of the cliff and colluvial slope (typically less than 0.5 m^2 in area) were scanned during each survey (fig. 2*B*). Small clusters of vegetation can create laser returns in front of the land surface and also create "shadows" of missing data on the land surface because the vegetation blocks the laser pulse from reaching the land surface. Additionally, erroneous multipath points (caused by a laser pulse bouncing off multiple objects before returning to the scanner) can be recorded. For each survey, the data were subdivided into small sections (3 m^2 each), and each section was individually inspected. Systematically inspecting the 3-m^2 areas ensured that points representing vegetation and other errant multipath laser returns were not included in the volume calculations.

Creating Surfaces

Volume was calculated by the PolyWorks® software package, which requires a continuous 3-D surface to be generated from the land-surface points. The randomly distributed land-surface points and areas of missing data (caused by vegetation shadows) were interpolated to create a continuous 3-D surface by a triangulated irregular network (TIN) of nearest neighbor points. This step was performed by the PolyWorks® software package.

Defining a Common Boundary

Prior to calculating the volume of sediment eroded or deposited, the area of the data common to all surveys was needed. This step eliminated any effect of areal sampling bias on the calculated differences in volume resulting from different extents of data in the surveys.

From a plan-view perspective, a common data boundary for the four surveys was defined across the top of the cliff and along the upstream and downstream margins. Along these boundaries, data for the four surveys were trimmed to match those of the survey with the least extent. Additional trimming across the base of the colluvial slope was necessary because of an abrupt change in grain-size distribution from very coarse gravel-sized clasts (32–64 mm in diameter) in the colluvial slope to cobble-sized clasts (64–256 mm in diameter) below it. Below this abrupt change across the base of the colluvial slope (figs. 2*B*, 5*A*), clasts finer than very coarse gravel had sifted into the interstitial spaces between the cobble-sized clasts and were no longer traceable with TLS for the purpose of volume calculations. The abrupt change in grain-size distribution coincided with the elevation of a high-water mark (HWM, or the flood-stage elevation) of the South Yuba River from December 2, 2012. The change in grain-size distribution and coincident HWM of the South Yuba River (figs. 2*B*, 4) collectively defined the lower elevation limit of the colluvial slope for the purpose of quantifying the volume of colluvial deposition, referred to as the base of the colluvial slope. The base of the colluvial slope slopes gently downstream from a horizontal perspective and undulates slightly in a plan-view perspective (figs. 2*B*, 4).

Defining Areas of Erosion and Deposition

In this study, the UCD KeckCAVES was used to identify the boundary (break in slope) between the base of the over-steepened slope and the top of the colluvial slope for each survey. The KeckCAVES was also used to define the base of the colluvial slope, described previously. Virtual-reality immersion in the 3-D point clouds, at a scale of approximately 1:1, allowed for precise identification and separation of the erosion (cliff and over-steepened slope) and deposition (colluvial slope) areas. The identification and separation of these areas was done for each survey because, in localized areas, the position of the undulating boundary varied slightly (up to several decimeters) between surveys. The aligned point clouds for each survey were trimmed to a common boundary for the cliff and over-steepened slope area and the colluvial slope area (Howle, 2019).

Calculating Volumes

The PolyWorks® software package was used to calculate the volume between a user-defined reference plane and the 3-D surfaces of the erosional area (cliff and over-steepened slope) and the depositional area (colluvial slope) for each survey, following methods described by Howle and others (2016). The volume calculations for each survey were made relative to a single fixed-reference plane that was oriented vertically and approximately parallel to the length of the cliff and colluvial slope. Using datasets for each area (erosional and depositional) and for each period, the volume between the fixed-reference plane and each 3-D surface was calculated perpendicular to the reference plane using a discretization interval of 1 square centimeter (cm^2). This discretization interval was applied across the entire extent of the cliff and colluvial-slope areas, which produced high-resolution surface-to-plane volume measurements of each area. The calculated volumetric changes were the differences in the measured volumes between sequential surveys.

Measurements of Sediment Density

Consolidated sediment that erodes from the cliff or over-steepened slope expands in volume as it falls, bounces, and rolls downslope before it is deposited on the colluvial slope below. The volumetric expansion is proportional to the difference in density of the eroded sediment of the cliff and over-steepened slope relative to that of the sediment deposited on the colluvial slope. To estimate the amount (mass) of sediment transported to below the base of the colluvial slope, the eroded and deposited volumes measured from the lidar data were multiplied by the corresponding sediment density, and the calculated eroded and deposited masses were differenced.

Three vertical transects for collection of samples for sediment-density measurements were established at the study site (fig. 4). Along each vertical transect, two samples each were collected from the cliff, the over-steepened slope, and the colluvial slope. The two samples from each area allowed for an assessment of the local variability in sediment density, and the three vertical transects allowed for a broader spatial assessment of the variability in sediment density. The samples were collected using a steel core barrel that was 13 cm long and had an inside diameter of 6.3 cm. A serrated cutting edge at the front end of the barrel was twisted and pushed into the sediment until the sediment filled the barrel. After the core barrel was removed from the sediment, the volume of sediment in the core barrel was measured in cubic centimeters (cm^3), and the sediment was weighed in grams (g). The moist bulk density of a sediment sample, in grams per cubic centimeter (g/cm^3), was calculated by dividing the mass by the volume. The calculated densities were moist bulk density measurements because no adjustments were made for moisture content of the cliff, over-steepened slope, or colluvial slope sediments. Sediment moisture content was assumed to be negligible for the purpose of assessing the density change related to sediment disaggregation. For details of the sediment density results, see appendix table 1–1.

The average moist bulk density of sediment from the cliff was 2.00±0.08 g/cm^3, and that of the over-steepened slope was 1.79±0.02 g/cm^3; thus, the average density of the sediment from the cliff and over-steepened slope areas was 1.89±0.09 g/cm^3 (table 1). The average moist bulk density of sediment deposited on the colluvial slope was 1.60±0.05 g/cm^3. The difference in density of sediment from the cliff and over-steepened slope areas compared with sediment on the colluvial slope, as a percentage, was calculated by dividing the average density of the eroded sediment (1.89 g/cm^3) by the average density of the colluvial slope sediment (1.60 g/cm^3). This equated to an average difference in sediment density of 18±1.8 percent (table 1).

Results of Volume Calculations

The calculated change in sediment volume (erosion and deposition measurements) for each period (December 2011 to October 2012, October 2012 to January 2013, and January 2013 to November 2013) is the difference between the measured volumes for the two surveys that bracket each period. The calculated volumes of sediment for each period (tables 2, 3) represent differences in the 3-D space between the cliff, over-steepened slope, and colluvial-slope surfaces in the surveys bracketing each period.

Table 1. Average moist bulk density of sediment from the cliff, over-steepened slope, and colluvial slope areas; average density of sediment from the cliff and over-steepened slope; and the average density difference, in percent, of sediment from the cliff and over-steepened slope areas compared to sediment from the colluvial slope.

[g/cm^3, grams per cubic centimeter; ±, plus or minus; —, not applicable]

Area	Average moist bulk density of sediment (g/cm^3)	Average density of cliff and over-steepened slope sediment (g/cm^3)	Percent difference of eroded sediment density compared to deposited sediment
Cliff	2.00±0.08	1.89±0.09	—
Over-steepened slope	1.79±0.02		—
Colluvial slope	1.60±0.05	—	18±1.8

Table 2. Calculated volumes between the surface of the cliff and over-steepened slope and reference planes for surveys 1, 2, 3, and 4.

[Volumes were calculated using the fixed-reference plane and reference planes orthogonally translated plus and minus 1 root-mean-square error (RMSE) of sequential alignments; volumes are relative to the indicated reference plane. **Abbreviations**: m^3, cubic meters; mm, millimeters; ±, plus or minus]

	Survey 1 (Dec. 15, 2011)	Survey 2 (Oct. 25, 2012)	Survey 3 (Jan. 4, 2013)	Survey 4 (Nov. 22, 2013)
Volume between fixed reference plane and surface of cliff and over-steepened slope (m^3)	12,100.0	12,117.8	12,235.1	12,309.3
Volume between reference plane, plus 1 RMSE, and surface of cliff and over-steepened slope (m^3)	—	12,114.6	12,231.9	12,305.2
Volume between reference plane, minus 1 RMSE, and surface of cliff and over-steepened slope (m^3)	—	12,121.0	12,238.3	12,313.4
Range of uncertainty, ±1 RMSE (m^3)	—	±3.2	±3.2	±4.1
Average erosion and range of uncertainty (m^3) between sequential surveys		17.8±3.2	117.3±6.4	74.2±7.3

Table 3. Calculated volumes between the colluvial slope surface and reference planes for surveys 1, 2, 3, and 4.

[Volumes were calculated using the fixed-reference plane and reference planes orthogonally translated plus and minus 1 root-mean-square error (RMSE) of sequential alignments; volumes are relative to the indicated reference plane. **Abbreviations**: m^3, cubic meters; mm, millimeters; —, not applicable; ±, plus or minus]

	Survey 1 (Dec. 15, 2011)	Survey 2 (Oct. 25, 2012)	Survey 3 (Jan. 4, 2013)	Survey 4 (Nov. 22, 2013)
Volume between fixed reference plane and surface of colluvial slope (m^3)	2,635.2	2,625.7	2,519.9	2,439.3
Volume between reference plane, plus 1 RMSE, and surface of colluvial slope (m^3)	—	2,624.2	2,518.3	2,437.2
Volume between reference plane, minus 1 RMSE, and surface of colluvial slope (m^3)	—	2,627.2	2,521.5	2,441.4
Range of uncertainty, ±1 RMSE (m^3)	—	±1.5	±1.6	±2.1
Average deposition and range of uncertainty (m^3) between sequential surveys		9.5±1.5	105.8±3.1	80.6±3.7

The RMSE of the sequential alignments relative to the baseline survey (4.5 mm for October 2012, 4.6 mm for January 2013, and 6.0 mm for November 2013) was used to assess potential volumetric errors. The assessment was made by translating the reference plane along an axis perpendicular to the reference plane by plus or minus the RMSE value and calculating surface-to-plane volumes for each reference plane position. Translating the reference plane by the RMSE in the positive direction (toward the cliff) resulted in a smaller calculated volume, whereas a negative RMSE translation (away from the cliff) resulted in a larger calculated volume (tables 2, 3). Alignment errors parallel to the reference plane did not change the calculated volume, and the largest potential errors resulted from misalignments perpendicular to the reference plane.

For each period, a range of erosional and depositional volumes was calculated as the difference between plus and minus 1 RMSE values derived from the associated alignment errors (tables 2, 3). For example, to estimate the maximum amount of erosion for October 2012 to January 2013, the October volume with a positive reference-plane error was subtracted from the January volume with a negative reference-plane error (table 2). Conversely, to estimate the minimum amount of erosion for October 2012 to January 2013, the October volume with a negative reference-plane error was subtracted from the January volume with a positive reference-plane error. Averages of the results of these combinations and the range of uncertainties are shown in tables 2 and 3 and are discussed next.

The range in the uncertainty values (plus or minus relative to the average) reflects the typical range of values likely to span the average value (tables 2, 3), and was derived from objective error assessments of the sequential alignments. The eroded and deposited volumes for each period were multiplied by the corresponding average sediment density resulting in a calculated mass (in kilograms) of eroded and deposited sediment (tables 4, 5). For each period, the mass of sediment deposited on the colluvial slope was subtracted from the mass of sediment eroded from the cliff and over-steepened slope areas to estimate the amount of sediment transported to below the base of the colluvial slope and the coincident HWM of the South Yuba River on December 2, 2012 (table 6).

Because some finer grained sediment could have lodged in the interstitial spaces between the cobble-sized clasts (below the base of the colluvial slope), the volume of deposited sediment and the corresponding calculated mass of deposited sediment, during each period, were potentially minimum values. A minimum estimate of deposited mass in a given period would, in turn, have caused the estimated mass of sediment transported below the base of the colluvial slope to be a maximum value.

During the first period, between the first survey (December 15, 2011) and second survey (October 25, 2012), 34±7 kilograms (kg) of mercury-contaminated sediment was eroded from the cliff and over-steepened slope areas at the study site. In the same period, 16±2 kg of sediment was deposited on the colluvial slope below the eroded area. The difference between the mass eroded and deposited was interpreted to indicate that 18±9 kg of sediment (table 6) was transported to an elevation below the base of the colluvial slope.

During the second period, between the second survey (October 25, 2012) and third survey (January 4, 2013), 221±22 kg of sediment was eroded from the cliff and over-steepened slope areas. During this same time frame, 170±9 kg of sediment was deposited on the colluvial slope. Again, the difference between the calculated eroded and deposited mass was interpreted to indicate that 51±31 kg of sediment (table 6) was delivered below the base of the colluvial slope and the coincident HWM from December 2, 2012.

Table 4. Measured volumes of erosion from the cliff and over-steepened slope, average density of eroded sediment, and calculated mass of sediment eroded from the cliff and over-steepened slope for three periods between surveys 1, 2, 3, and 4 and for the overall period between surveys 1 and 4.

[g/cm^3, grams per cubic centimeter; kg, kilograms; m^3, cubic meters; Survey 1, December 15, 2011; Survey 2, October 25, 2012; Survey 3, January 4, 2013; and Survey 4, November 22, 2013; ±, plus or minus]

Bracketing surveys	Erosion volume from cliff and over-steepened slope and range of uncertainty (m^3)	Average density of eroded sediment and range of uncertainty (g/cm^3)	Mass of sediment eroded from cliff and over-steepened slope and range of uncertainty (kg)
Survey 1–Survey 2 (315 days)	18±3.2	1.89±0.09	34±7
Survey 2–Survey 3 (71 days)	117±6.4	1.89±0.09	221±22
Survey 3–Survey 4 (322 days)	74±7.3	1.89±0.09	140±18
Total of Surveys 1 through 4 (708 days)	209±16.9	1.89±0.09	395±46

Table 5. Measured volumes of deposition on the colluvial slope, average density of deposited sediment, and calculated mass of sediment deposited on the colluvial slope for three periods between surveys 1, 2, 3, and 4 and for the overall period between surveys 1 and 4.

[g/cm^3, grams per cubic centimeter; kg, kilograms; m^3, cubic meters; Survey 1, December 15, 2011; Survey 2, October 25, 2012; Survey 3, January 4, 2013; and Survey 4, November 22, 2013; ±, plus or minus]

Bracketing surveys	Deposition volume on colluvial slope and range of uncertainty (m^3)	Average density of deposited sediment and range of uncertainty (g/cm^3)	Mass of sediment deposited on the colluvial slope and range of uncertainty (kg)
Survey 1–Survey 2 (315 days)	10±1.5	1.60±0.05	16±2
Survey 2–Survey 3 (71 days)	106±3.1	1.60±0.05	170±9
Survey 3–Survey 4 (322 days)	81±3.7	1.60±0.05	130±8
Total of Surveys 1 through 4 (708 days)	197±8.3	1.60±0.05	316±20

Table 6. Estimated mass of sediment transported into an elevation zone below the base of the colluvial slope for three periods between surveys 1, 2, 3, and 4 and for the overall period between surveys 1 and 4.

[kg, kilograms; Survey 1, December 15, 2011; Survey 2, October 25, 2012; Survey 3, January 4, 2013; and Survey 4, November 22, 2013; ±, plus or minus]

Bracketing surveys	Mass of eroded sediment and range of uncertainty (kg)	Mass of deposited sediment and range of uncertainty (kg)	Estimated mass of sediment transported below base of the colluvial slope and range of uncertainty (kg)
Survey 1–Survey 2 (315 days)	34±7	16±2	18±9
Survey 2–Survey 3 (71 days)	221±22	170±9	51±31
Survey 3–Survey 4 (322 days)	140±18	130±8	10±26
Total of Surveys 1 through 4 (708 days)	395±46	316±20	79±66

During the final period, between the third survey (January 4, 2013) and the fourth survey (November 22, 2013), an additional 140±18 kg of sediment was eroded from the cliff area. During this period, 130±8 kg of sediment was deposited on the colluvial slope, indicating that 10±26 kg of sediment was transported below the base of the colluvial slope.

Combining the calculated mass from the three periods between the four surveys (December 15, 2011–November 22, 2013), the total mass of sediment eroded from the cliff and over-steepened slope was 395±46 kg. During this same period, 316±20 kg of sediment was deposited on the colluvial slope. These values yielded an estimated 79±66 kg of mercury-contaminated sediment transported to below the base of the colluvial slope and the HWM from December 2, 2012 (table 6). The period when the majority of sediment was moved by erosion and deposition was between Survey 2 and Survey 3 (which included an atmospheric river rain event of 4 days that ended on December 2, 2012), when an estimated 51±31 kg of sediment (about 64 percent of the total) was transported to below the base of the colluvial slope.

Visualization of Land-Surface Changes

In this section, two-dimensional (2-D) change plots, which allow for the visualization of where, when, and how much the land surface changed in the study area, are presented. The graphics facilitate the interpretation of the geomorphic and hydrologic processes responsible for the changes and provide a basis for determining where mitigation measures, if deemed necessary, would be most effective.

Color-coded 2-D change plots were created in PolyWorks® by measuring the distance between the surfaces defined from sequential surveys. To emphasize the primary direction of change across the cliff and over-steepened slope, the differences in sequential data were calculated for the horizontal direction; for the colluvial slope, differences in the data were calculated for the vertical direction. These change plots show the amount and spatial variability of land-surface change across the study area between sequential surveys (figs. 6, 7, 8) and for the entire period of the study (fig. 9). These images also demonstrate the spatial resolution of the TLS data.

Between the first and second surveys (from December 15, 2011, to October 25, 2012), erosion was widespread across the cliff and over-steepened slope areas (fig. 6*A*), although there were also localized areas of deposition. The broad extent of green in figure 6*A* shows areas of minimal erosion ranging from 0 to approximately 0.08 m of horizontal change; the yellow areas represent horizontal change of approximately 0.08 to 0.15 m, the orange areas indicate erosion of about 0.20 m, and the discrete areas of red represent localized erosion of up to 0.30 m. The patches of light to dark blue in figure 6*A* represent local areas where sediment was deposited. For the same time period, the color distribution across the colluvial slope is in the opposite direction (compare fig. 6*B* to fig. 6*A*), with widespread aggradation across the colluvial slope (blue areas) and only localized areas of degradation (yellow and red areas). In the central part of the cliff, figure 6*A* shows a linear swath of concentrated erosion of approximately 0.10–0.30 m (horizontal change) along a broad gully. Directly below that gully, at the base of the colluvial slope, there was a conical shaped area (fig. 6*B*) indicating deposition up to about 0.40 m (vertical change).

Between the second and third surveys (from October 25, 2012, to January 4, 2013), a large amount of precipitation associated with an atmospheric river (AR) fell in late November and early December 2012. During the 4 days from November 29 through December 2, 2012, the NWS station at Grass Valley, Calif., recorded 0.289 m (11.4 in.) of rain, which caused substantial erosion and deposition at the Humbug Creek study site and also produced high streamflow (flood stage) in the South Yuba River. Although the 71 days of this period was only 10 percent of the entire study (December 15, 2011, to November 22, 2013, or 708 days), the precipitation associated with the AR caused the largest volume and mass changes of the study (tables 4–6).

The cliff and over-steepened slope areas shown in figure 7*A* are speckled with numerous zones of red color, which grade outward into halos of orange to yellow colors, indicating localized patches of erosion ranging from a maximum horizontal change of approximately 0.40 m (red) in the center to approximately 0.15 m (yellow) near the edges. Although the erosion pattern appears to be mostly random, there are swaths indicating erosion (red to yellow colors) aligned in a downslope direction (fig. 7*A*). These linear swaths originated from broad alcoves at the top of the cliff. This pattern indicates that sheet wash coalesced in gullies on the moderately indurated sediments of the cliff and over-steepened slope areas. Near the top of the cliff, in the western half of figure 7*A*, there is an approximately 2.5-m-wide area of orange to red color indicating erosion of 0.35–0.40 m. This relatively deep and isolated erosion is interpreted to have formed by the detachment and collapse of a coherent block of sediment from an overhanging section of the cliff. Visual inspection of this area at the time of the third survey confirmed an overhanging roof above the deep recess. Also evident in figure 7*A* are areas of aggradation (blue colors), most notably on the western side of the over-steepened slope. Curiously, the areas upslope from these areas of aggradation show only minor erosion (green) during this period. A possible interpretation of this is that overland flow from above the cliff might have washed sediment over the cliff during the AR, resulting in deposition on top of cobbles protruding from the cliff face and on the over-steepened slope below the cliff. It is also worth noting that the third survey was the only one of the four that was done during winter conditions, when higher moisture content may cause seasonal swelling of clay minerals, with an unknown effect on topography.

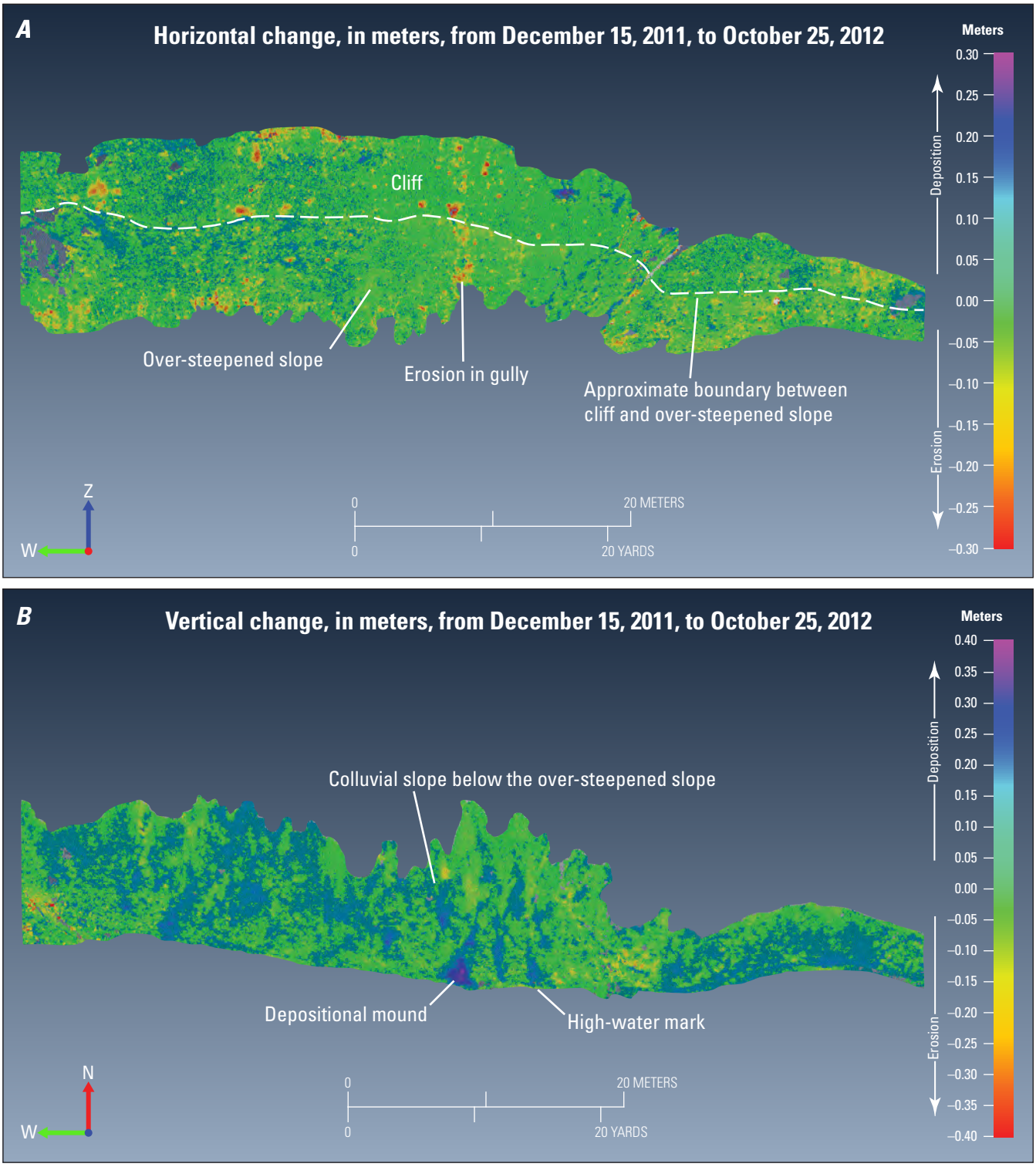

Figure 6. Erosional and depositional changes in land surface at the confluence of the South Yuba River and Humbug Creek from December 15, 2011, to October 25, 2012: *A*, horizontal change across the cliff and over-steepened slope areas. Gray areas represent missing or sparse lidar data density that did not allow for a difference to be calculated; *B*, vertical change across the colluvial slope.

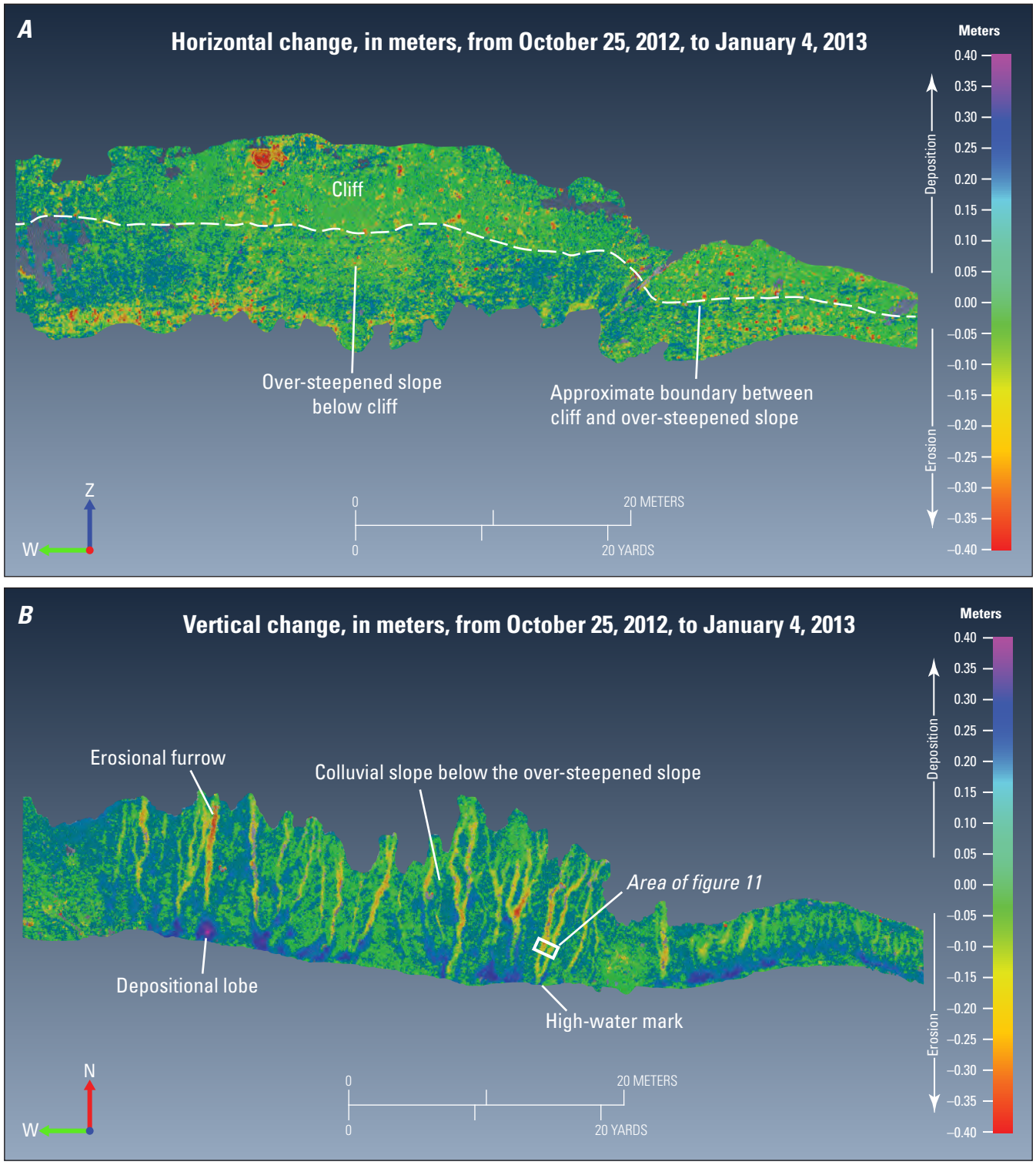

Figure 7. Erosional and depositional changes in land surface at the confluence of the South Yuba River and Humbug Creek from October 25, 2012, to January 4, 2013: *A*, horizontal change across the cliff and over-steepened slope areas. Gray areas represent missing or sparse lidar data density that did not allow for a difference to be calculated; *B*, vertical change across the colluvial slope.

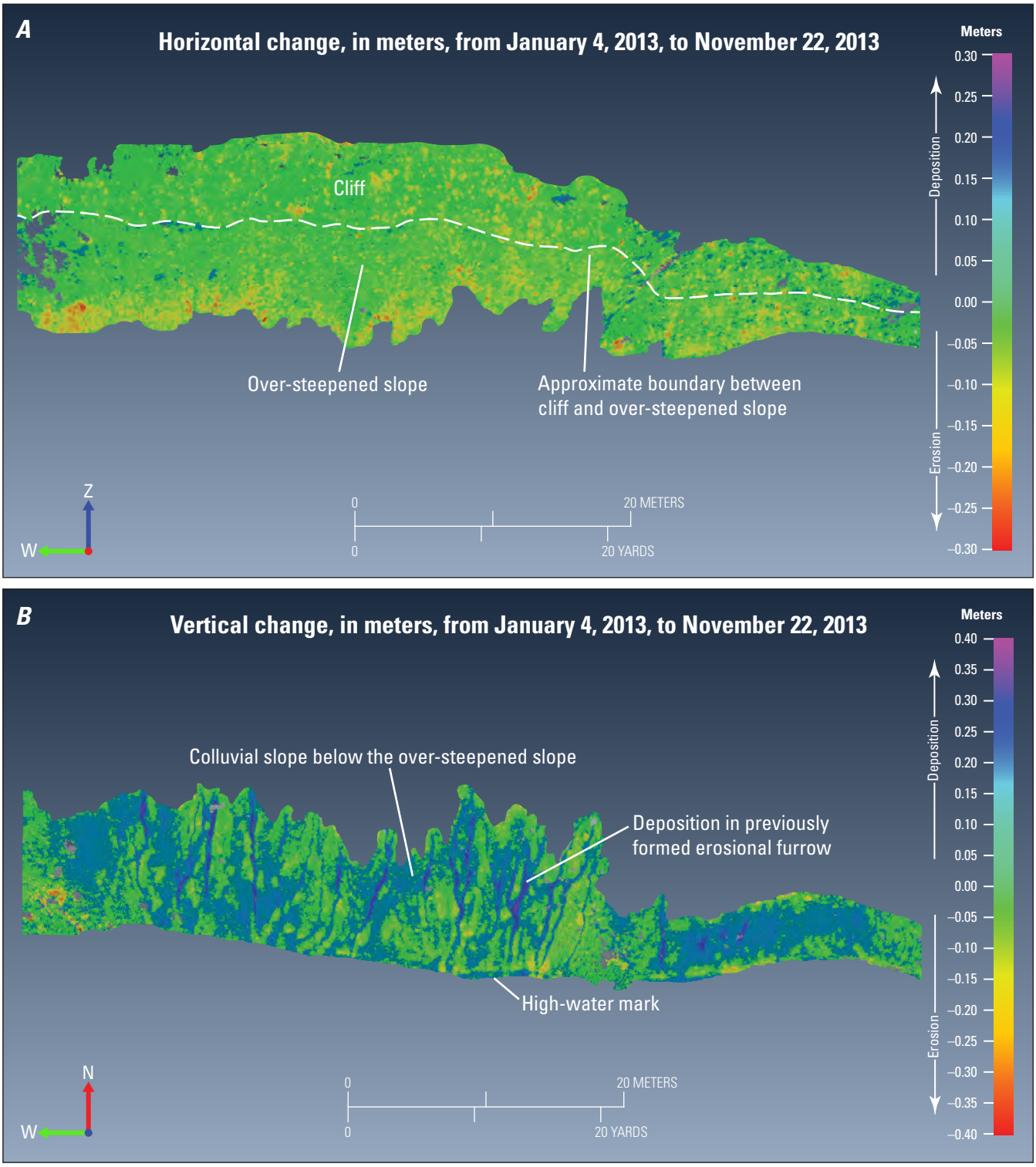

Figure 8. Erosional and depositional changes in land surface at the confluence of the South Yuba River and Humbug Creek from January 4, 2013, to November 22, 2013: *A*, horizontal change across the cliff and over-steepened slope areas. Gray areas represent missing or sparse lidar data density that did not allow for a difference to be calculated; *B*, vertical change across the colluvial slope.

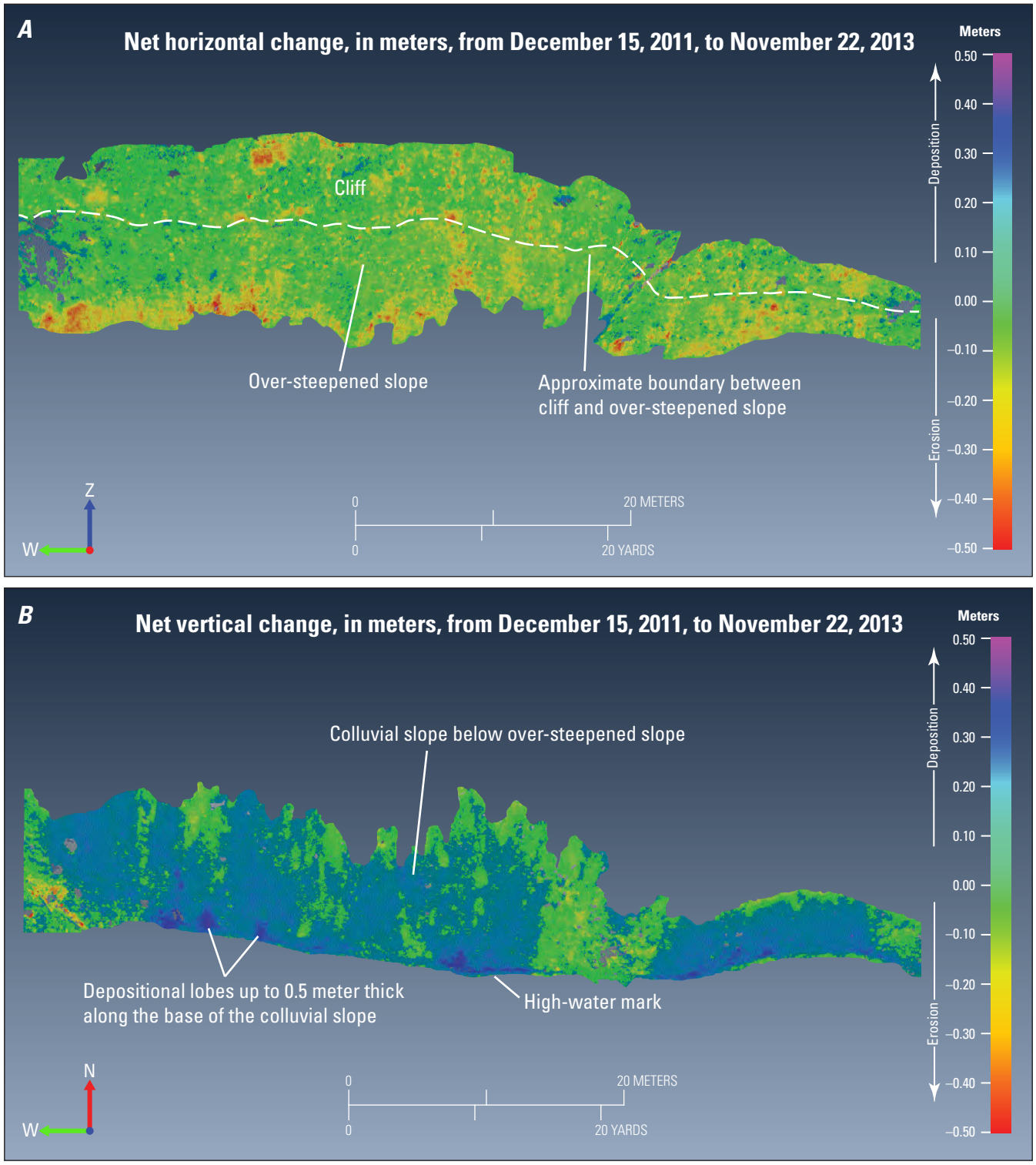

Figure 9. Erosional and depositional changes in land surface at the confluence of the South Yuba River and Humbug Creek from December 15, 2011, to November 22, 2013: *A*, horizontal change across the cliff and over-steepened slope areas. Gray areas represent missing or sparse lidar data density that did not allow for a difference to be calculated; *B*, vertical change across the colluvial slope.

On the colluvial slope, channelized flow incised numerous furrows (up to 0.40 m deep and 1.0 m wide) in the unconsolidated colluvium (figs. 7*B*, 10). These erosional furrows were aligned with erosional areas on the over-steepened slope above (fig. 7*A*), indicating the coalescence and channelization of sheet wash during the AR. Directly below the erosional furrows were depositional lobes of sediment ranging from 0.20 to 0.40 m in height and several meters in width. The channelization of sheet wash in the furrows appears to have generated debris flows, or the rapid downslope transport of water-saturated sediment. This is indicated by lateral levees flanking the lower parts of the incised furrows and the upward coarsening of sediment deposited in the terminal lobes (fig. 10). Adjacent to the incised furrows and across much of the colluvial slope were areas of moderate deposition (fig. 7*B*), ranging from 0.10–0.15 m (light blue) to 0.20–0.25 m (blue).

An example of the juxtaposition of deposition and erosion on the colluvial slope from the October 2012 to January 2013 period is illustrated in figure 11 for a selected area of the colluvial slope (see figs. 7*B* and 10*A* for location). Figure 11*A* shows the point-cloud data for the October 2012 and January 2013 surveys from an oblique perspective (looking up and parallel to the colluvial slope). The October 2012 data (blue lidar points in fig. 11*A*) indicated a relatively smooth colluvial-slope surface. In contrast, the January 2013 data (yellow lidar points) were both above and below the October 2012 surface. The areas of yellow (October 2012) data above the blue (January 2013) data indicate localized deposition up to 0.10 m on the October 2012 surface. The most logical interpretation of this is that deposition was followed by a period of erosion. The channelization of sheet wash from the cliff and over-steepened slope areas incised (eroded) the colluvial-slope surface to form erosional furrows (figs. 7*B*, 10*A*). Figure 11*B* shows the amount of deposition and erosion (vertical change) for the selected area. In the selected area, the maximum deposition relative to the October 2012 surface was about 0.10 m (pink area), whereas the maximum erosion was 0.25 m (red area).

During the final period of this study, between the third and the fourth surveys (January 4, 2013, to November 22, 2013), erosion was moderate across the cliff and over-steepened slope areas (fig. 8*A*). The broad extent of green in figure 8*A* represents areas of minimal erosion during this period, ranging from 0 to approximately 0.08 m of horizontal change; the yellow areas represent horizontal change of approximately 0.10 to about 0.15 m, except for discrete areas of red, primarily along the lower margin of the over-steepened slope, of localized erosion of up to 0.30 m. During this period, across the colluvial slope, there was widespread deposition of 0.15–0.20 m (light blue to blue in fig. 8*B*), except in the previously formed furrows, which were in-filled with 0.30–0.40 m (purple to pink in fig. 8*B*) of sediment from upslope areas.

The net horizontal and vertical differences between the first survey (December 15, 2011) and the final survey (November 22, 2013) are shown in figure 9. Across the cliff and over-steepened slope areas, light green to yellow colors indicate that there was widespread erosion, ranging from approximately 0.10 to 0.25 m of horizontal change. In addition, there are numerous patches of orange color that grade inward to red. In these localized areas, horizontal erosion from 0.30 m (orange) to a maximum of 0.50 m (red) occurred during the study period. As previously discussed, in several locations across the cliff and over-steepened slope areas, there are swaths of erosional zones (red to yellow colors in fig. 9*A*) aligned in a downslope direction. These linear swaths, which originated from broad alcoves at the top of the cliff, indicate that sheet wash coalesced and concentrated erosion in shallow gullies in the cliff and over-steepened slope areas.

Across the base of the colluvial slope are numerous depositional lobes indicated by the blue to purple colors (fig. 9*B*). This color gradation depicts vertical aggradation that ranged from approximately 0.25 m (blue) up to a maximum of 0.50 m (purple). These areas of maximum deposition were roughly aligned with the linear swaths of erosion in the cliff and over-steepened slope areas above. Elsewhere across the colluvial slope, the light blue to blue colors represent the widespread vertical accumulation of sediment that ranged from approximately 0.15 to 0.25 m (fig. 9*B*).

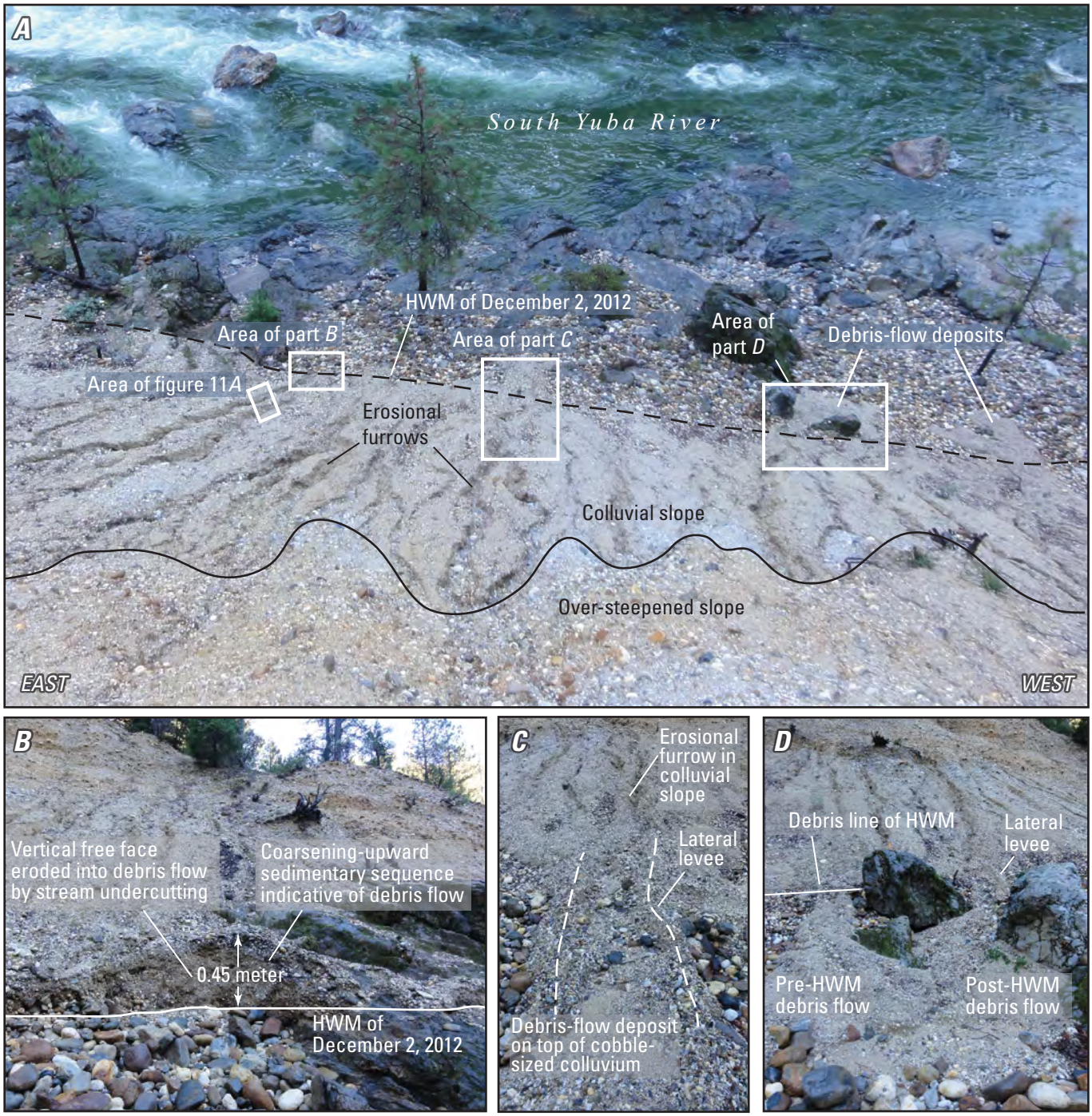

Figure 10. South Yuba River–Humbug Creek study site on December 11, 2012: *A*, Oblique photograph taken from the top of the cliff (looking down) showing erosional furrows, debris-flow deposits, and the high-water mark (HWM) of the South Yuba River from December 2, 2012; *B*, vertical free face eroded into debris-flow deposit, upward-coarsening sedimentary sequence in vertical free face, and HWM from December 2, 2012, at the base of the vertical free face; *C*, erosional furrow, debris-flow deposit, and lateral levees flanking debris flow; and *D*, HWM debris line and debris flows deposited before and after the December 2, 2012, HWM. Photographs taken December 11, 2012.

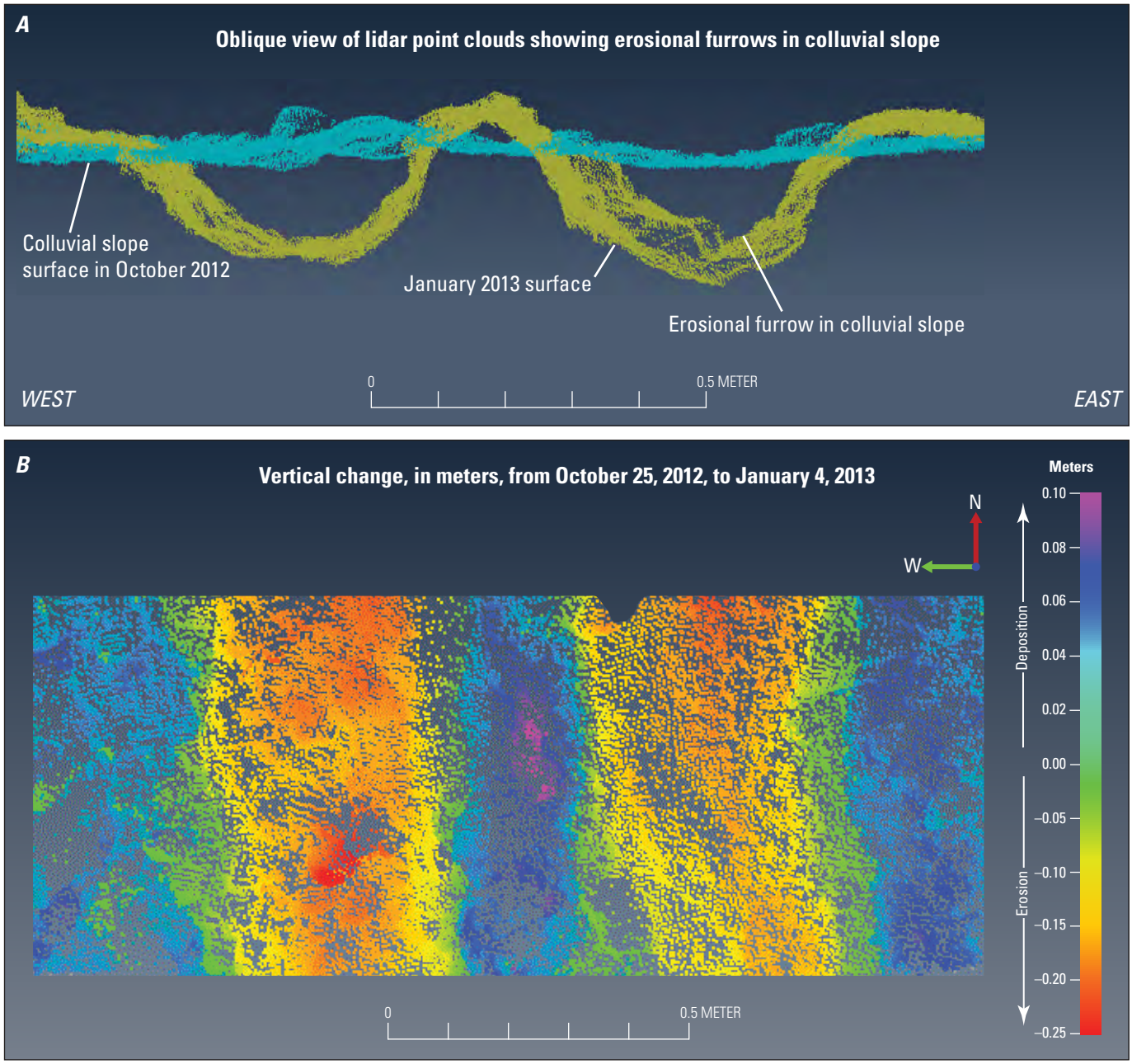

Figure 11. Oblique view of a selected area of the colluvial slope and erosional and depositional changes from October 25, 2012, to January 4, 2013 (see figs. 7*B* and 10*A* for the location of the selected area): *A*, oblique view (looking up and parallel to the colluvial slope) of lidar point clouds for October 2012 and January 2013; *B*, plan view of vertical change across the colluvial slope.

Estimation of Flood Annual Exceedance Probabilities

In this section, annual exceedance probabilities (AEP) of floods and associated river stages (water-surface elevations) are estimated to assess how frequently the colluvial slope at the study site could be inundated by the South Yuba River. These estimates can also help determine how much of the mercury-contaminated sediment in the colluvial-slope area might be mobilized by the South Yuba River during floods.

Peak Discharge of December 2, 2012 (Atmospheric River)

The AR precipitation from November 29 to December 2, 2012, generated a total of 0.289 m (11.4 in.) of precipitation at the NWS station in Grass Valley, Calif., with 37 percent (0.106 m or 4.2 in.) of the total falling on December 2, 2012, alone. The high-intensity, short duration AR precipitation produced a peak-flow discharge of 18,700 cubic feet per second (ft^3/s) in the South Yuba River at Jones Bar streamflow gage (USGS site-identification number 11417500, fig. 1), 16 km west-southwest (downstream) of the Humbug Creek study site. The peak discharge at the Jones Bar streamflow gage on December 2, 2012, was most likely greater than the peak-flow discharge at the Humbug Creek study site because of the additional contributing drainage area downstream from the study site. Using the USGS StreamStats application (http://water.usgs.gov/osw/streamstats/index.html), the drainage area (DA) ratio was determined to be 0.87. This ratio relates the approximately 267 square miles (mi^2) of drainage area upstream from the study site to the total South Yuba River drainage area (308 mi^2), which is equivalent to 87 percent of the total drainage area (267 divided by 308). Although the upper part of the watershed is partially regulated by Lake Spaulding, any effects the reservoir has on peak flows in the watershed should be captured in the flow data at the Jones Bar gage, which was installed after the reservoir was built. Using the DA ratio (0.87) and relations developed by Berenbrock (2002), the December 2, 2012, peak flow at the Humbug Creek study site was estimated to have been approximately 16,300 ft^3/s.

Estimation of Annual Exceedance Probabilities

An AEP analysis of the long-term discharge record at the Jones Bar streamflow gage (dating from 1940) was done to estimate the recurrence interval of floods having a magnitude equal to the December 2, 2012, flood. Using the USGS PeakFQ program (Veilleux and others, 2014) and regional regression equations (Gotvald and others, 2012; Lamontagne and others, 2012), the December 2, 2012, flood was determined to have had an AEP between 10 percent (22,700 ft^3/s) and 20 percent (15,400 ft^3/s) at the Jones Bar streamflow gage. This means that in any given year, there is a 10–20 percent chance (10- and 5-year recurrence intervals, respectively) of a flood equal to or greater than that of December 2, 2012, that is capable of mobilizing mercury-contaminated sediment at the study site into the South Yuba River. The regional regression equations of Gotvald and others (2012) were also used to estimate the discharge of floods for the 1- and 2-percent AEP (100- and 50-year recurrence intervals, respectively) at the Jones Bar streamflow gage. The discharge of a 100-year recurrence-interval flood at Jones Bar was estimated to be 54,800 ft^3/s, and the 50-year flood was estimated to be 43,800 ft^3/s (table 7).

The discharges for the 5-, 10-, 50-, and 100-year recurrence-interval floods at the Jones Bar streamflow gage were adjusted for the difference in contributing drainage area at the Humbug Creek study site compared to Jones Bar to estimate the discharge of these various floods at the study site (table 7). The peak-flow discharges for the 5-, 10-, 50-, and 100-year recurrence-interval floods at the South Yuba River–Humbug Creek confluence study site are listed in table 7, as well as the associated lower and upper 95-percent confidence limits.

Table 7. Flood annual exceedance probabilities for the South Yuba River at Jones Bar and the South Yuba River downstream from the Humbug Creek confluence, corresponding recurrence intervals, peak flows, lower and upper 95-percent confidence limits, and river stage relative to the December 2, 2012, peak flow.

[ft^3/s, cubic feet per second; m, meters]

Flood annual exceedance probability (percent)	Flood recurrence interval (years)	South Yuba River at Jones Bar	South Yuba River at study site				
		Peak flow (ft^3/s)	Peak flow (ft^3/s)	95-percent confidence lower (ft^3/s)	95-percent confidence upper (ft^3/s)	River stage relative to Dec. 2, 2012, peak (m)	River stage uncertainty 95-percent confidence limits (m)
20	5	15,400	13,400	10,400	17,200	–0.4	–0.9, 0.1
10	10	22,700	19,700	15,000	26,100	0.4	–0.2, 1.1
2	50	43,800	38,100	25,400	57,100	2.2	1.0, 3.6
1	100	54,800	47,700	29,800	76,400	3.0	1.5, 4.9

Stage-Discharge Rating

A stage-discharge rating for the South Yuba River–Humbug Creek study site was developed so that the gaged streamflow at Jones Bar could be related to a stage at the study site. The December 2, 2012, peak reached the base of the colluvial slope and defined the minimum discharge at the Jones Bar gage required to mobilize mercury-contaminated sediment at the study site. An upward extension of the stage-discharge rating at the study site allowed for estimates of how much of the colluvial slope would be likely to be inundated by 50- and 100-year recurrence-interval floods.

Four USGS crest-stage gages (CSG) were established at the study site to record high-water stages (peaks), which were related to the gaged streamflow downstream at Jones Bar. The corresponding peak flows at Jones Bar were adjusted to account for the difference in intervening drainage area, as previously discussed, to estimate the streamflow at the study site. Coupled pairs of CSG-recorded stage and drainage-area-adjusted discharge from three high-water peaks (the December 2, 2012, peak and two smaller peaks) were used to define a linear (log-log scale) stage-discharge rating for the South Yuba River–Humbug Creek study site. A stage of 0.0 at the South Yuba River–Humbug Creek study site was equivalent to the December 2, 2012, peak. This numerical stage-discharge rating included stream discharge up to 16,300 ft^3/s (December 2, 2012, peak). This rating was extended (linearly) to estimate the corresponding stages of the 1- and 2-percent AEP floods at the study site, which were 47,700 and 38,100 ft^3/s, respectively (table 7).

Step-Backwater Analysis

The USGS did a step-backwater survey of the South Yuba River channel for the stream reach by and upstream from the study site (fig. 2*A*). The purpose of the step-backwater survey and subsequent computation was to provide a quality-assurance check of the river stages estimated for the 50- and 100-year recurrence interval floods determined from the rating extension, previously discussed. Techniques for the survey and computation of the step-backwater method are described by Davidian (1984) and use channel cross-section geometry, channel slope, and surface roughness to estimate the water-surface profile for a given discharge.

A total of 10 channel cross-sections were surveyed over a 280-m-long reach of the South Yuba River (fig. 2*A*) to define the channel geometry. A Manning's 'n' value of 0.070 was used as an estimate of the channel roughness based on visual analysis of the channel and comparison with published Manning's 'n' values (Barnes, 1967). A channel slope of 0.010 was used as the downstream boundary condition based on analysis of the surveyed cross-section data and surveyed HWMs from an earlier flood (assumed to be the most recent flood of January 1997 based on the appearance of the HWMs). The surveyed channel geometry and roughness value were entered in HEC-RAS, a flow-modeling program developed by the U.S. Army Corps of Engineers (2010). The HEC-RAS program was used as a one-dimensional, steady-flow model to estimate the water-surface elevations for discharges associated with the 1- and 2-percent annual exceedance probability flood estimates. The results were within 0.1 meter of those determined from the rating extension, indicating that the field measurements and related assumptions were reasonable.

Channel roughness and slope were varied to test the sensitivity of the modeled results to differences in these subjective input parameters. A 10-percent increase or decrease in Manning's 'n' resulted in an approximate ±0.4 m difference in stage values for the 1- and 2-percent AEP (50- and 100-year recurrence interval) floods, whereas a 10-percent increase or decrease in channel slope resulted in a ±0.2-m difference in the stage values for the same floods.

Colluvial-Slope Inundation

Relating the 1- and 2-percent AEP peak-flow discharge at the study site to river stage provides estimates of how much of the colluvial slope could be inundated during either a 50- or 100-year recurrence-interval flood. For the 50-year flood, the extended stage-discharge rating indicated that the lower 2.2 m of the colluvial slope could be inundated, with a 95-percent confidence interval of stages ranging from 1.0 to 3.6 m above the December 2, 2012, stage (table 7). The 100-year flood could inundate an additional 0.8 m of the colluvial-slope sediment, or a stage of 3.0 m, with a 95-percent confidence interval range of stages from 1.5 to 4.9 m above the December 2, 2012, HWM (table 7). If realized, these high river stages could inundate the lower half of the colluvial slope and thereby substantially increase the mobilization of mercury-contaminated sediment from the Humbug Creek study site to downstream areas.

Summary

Substantial quantities of mercury were used and lost to the environment from historical placer gold mining activities on the western slope of the Sierra Nevada, California, and recent studies have documented continued persistence of mercury and methylmercury concentrations in water, sediment, fish, and predatory invertebrates in the Yuba River drainage basin in relation to suspected mercury sources. To identify areas that have high levels of mercury contamination as possible remediation targets in the Yuba River drainage basin and other areas in the Sierra Nevada, the U.S. Geological Survey (USGS) worked in cooperation with the Bureau of Land Management (BLM) on this and other detailed studies. The study site is at the confluence of Humbug Creek and the South Yuba River, approximately 17 kilometers northeast of Grass Valley, Nevada County, California. One of the largest hydraulic gold mines in the Sierra Nevada is 3.5 kilometers north of the study site in the Humbug Creek subbasin.

This report documents methods and results of a time series of terrestrial laser scanning (TLS) of an eroding outcrop of mercury-contaminated sediment near the confluence of Humbug Creek and the South Yuba River. Specifically, this report (1) documents the methods used to quantify the volume of sediment eroded from the cliff and over-steepened areas and deposited on the colluvial slope below; (2) estimates the incremental and total mass of sediment delivered below a historical flood stage for three periods between December 15, 2011, and November 22, 2013; (3) presents a flood annual exceedance probability for a South Yuba River flood that is equal to the flood of December 2, 2012; and (4) provides estimates of how much of the mercury-contaminated sediment on the colluvial slope could be inundated by floods at the 1- and 2-percent annual exceedance probability (100- and 50-year recurrence interval floods, respectively).

Sequential TLS was an effective tool to quantify the volumetric changes of a complex, eroding surface that could not be mapped by traditional surveying techniques. The non-destructive scanning of the sediments and sub-centimeter resolution of the resulting point clouds allowed for a spatially detailed assessment of change across the cliff, over-steepened slope, and colluvial slope areas. In this study, each of these areas was surveyed four times using TLS. Each survey was composed of six TLS scans collected from different vantages that were combined in a composite three-dimensional (3-D) point cloud of the study site. The sequential surveys were co-registered, or 'aligned,' in a common 3-D reference frame so that volumetric comparisons between the surveys could be made. The use of virtual reality technology enabled a 3-D inspection of the alignments of the lidar point-cloud data and separation of the data subsets for cliff and colluvial slope areas more intuitively, quickly, and accurately than previously possible with non-immersive two-dimensional (2-D) environments, greatly increasing the level of confidence in data quality and data analysis.

For each survey, a volume for the erosional area (cliff and over-steepened slope areas) and for the depositional area (colluvial slope area) was computed between a common reference plane and the surveyed land surface. Volumetric differences from cliff and over-steepened slope erosion and colluvial slope deposition were calculated for each between-survey period (December 2011 to October 2012, October 2012 to January 2013, and January 2013 to November 2013), as the difference between measured volumes for the two surveys that bracketed a given period. The calculated volumes of sediment, for the erosional and depositional areas, represented the 3-D space between the respective surfaces from the bracketing surveys.

The eroded and deposited volumes for each period were multiplied by the corresponding average sediment density resulting in a calculated mass of eroded and deposited sediment. For each period, the mass of sediment deposited on the colluvial slope was subtracted from the mass of sediment eroded from the cliff and over-steepened slope areas to estimate the amount of sediment transported below the base of the colluvial slope—the level coincident with the high-water mark (HWM) of the South Yuba River on December 2, 2012. Because some finer grained sediment could have lodged in the interstitial spaces between the cobble-sized clasts (below the base of the colluvial slope), the volumes of deposited sediment and the corresponding calculated mass of deposited sediment, during each period, were potentially minimum values. A minimum estimate of deposited mass in a given period would, in turn, have caused the estimated mass of sediment transported below the base of the colluvial slope to be a maximum value.

For the first period, between the first survey (December 15, 2011) and second survey (October 25, 2012), 34±7 kilograms (kg) of sediment was eroded from the cliff and over-steepened slope area at the Humbug Creek study site. In the same period, 16±2 kg of sediment was deposited on the colluvial slope below. The difference between these calculated masses indicated an estimated 18±9 kg of mercury-contaminated sediment was transported to below the base of the colluvial slope.

During the second period, between the second survey (October 25, 2012) and third survey (January 4, 2013), precipitation during an atmospheric river storm event caused substantial erosion and deposition at the Humbug Creek study site and also produced a high streamflow (flood stage) in the South Yuba River. During this period, 221±22 kg of sediment was eroded from the cliff and over-steepened slope area. During the same period, 170±9 kg of sediment was deposited on the colluvial slope, indicating that 51±31 kg of sediment was transported below the base of the colluvial slope and the coincident HWM of the South Yuba River from December 2, 2012. Although this second period was the shortest period (71 days) of the entire December 15, 2011, to November 22, 2013, study period (708 days), erosion during the atmospheric river produced the largest changes in volume and mass of sediment of the entire study.

In the final period, between the third survey (January 4, 2013) and the fourth survey (November 22, 2013), 140±18 kg of sediment was eroded from the cliff and over-steepened slope area. During this period, 130±8 kg of sediment was deposited on the colluvial slope, indicating that 10±26 kg was transported below the base of the colluvial slope.

The sum of the calculated masses for the three periods between the four surveys (from December 15, 2011, through November 22, 2013) indicated the total mass of sediment eroded from the cliff and over-steepened slope area was 395±46 kg. During the entire study period, a total 316±20 kg of sediment was deposited on the colluvial slope. These values indicated an estimated 79±66 kg of sediment was transported below the base of the colluvial slope and the South Yuba River HWM of December 2, 2012.

The South Yuba River flood on December 2, 2012, approximated the minimum flood required to mobilize mercury-contaminated sediment at the study site and had an annual exceedance probability between 10 and 20 percent (recurrence interval of 5–10 years). Floods having 1- and 2-percent annual exceedance probabilities (recurrence intervals of 100 and 50 years, respectively) could inundate the lower half of the colluvial slope and thereby substantially increase the mobilization of mercury-contaminated sediment from the Humbug Creek study site to downstream areas.

The results of this study, combined with laboratory data regarding mercury concentration and grain-size distribution that could be publicly available at a future date, could make it possible to quantify the amount of mercury eroded into the South Yuba River during the study period. Results from these investigations are for use by the BLM, in consultation with other federal, state, and local agencies, as well as other interested parties, to determine whether removal or stabilization of mercury-contaminated sediment could be needed at the South Yuba River–Humbug Creek study site. These results can be used by the BLM to prioritize remediation activities related to abandoned mines and mine wastes in the South Yuba River drainage basin.

References Cited

Alpers, C.N., 2017, Arsenic and mercury contamination related to historical gold mining in the Sierra Nevada, California: Geochemistry: Exploration, Environment, Analysis, v. 17, p. 92–100, http://geea.lyellcollection.org/content/17/2/92.

Alpers, C.N., Hunerlach, M.P., May, J.T., and Hothem, R.L., 2005a, Mercury contamination from historical gold mining in California: U.S. Geological Survey Fact Sheet 2005–3014, 6 p., https://doi.org/10.3133/fs20053014.

Alpers, C.N., Hunerlach, M.P., May, J.T., Hothem, R.L., Taylor, H.E., Antweiler, R.C., De Wild, J.F., and Lawler, D.A., 2005b, Geochemical characterization of water, sediment, and biota affected by mercury contamination and acidic drainage from historical gold mining, Greenhorn Creek, Nevada County, California, 1999–2001: U.S. Geological Survey Scientific Investigations Report 2004–5251, 278 p., https://doi.org/10.3133/sir20045251.

Alpers, C.N., Hunerlach, M.P., Marvin-DiPasquale, M.C., Antweiler, R.C., Lasorsa, B.K., De Wild, J.F., and Snyder, N.P., 2006, Geochemical data for mercury, methylmercury, and other constituents in sediments from Englebright Lake, California, 2002: U.S. Geological Survey Data Series 151, 95 p., https://doi.org/10.3133/ds151.

Alpers, C.N., Fleck. J.A., Beaulieu, E., Hothem, R.L., May, J.T., Marvin-DiPasquale, M., Blum, A.E., and Graves, P.G., 2012, Characterization of mercury and methylmercury contamination in stream and pond environments and provenance of mine waste from historical gold mining in the Sierra Nevada, California [abs.], *in* U.S. Environmental Protection Agency Hardrock Mining Conference 2012, Advancing solutions for a new legacy: Denver, Colo., April 3–5, 2012, p. 105.

Alpers, C.N., Yee, J.L., Ackerman, J.T., Orlando, J.L., Slotton, D.G., and Marvin-DiPasquale, M., 2016, Prediction of fish and sediment mercury in streams using landscape variables and historical mining: Science of the Total Environment, v. 571, p. 364–379, https://doi.org/10.1016/j.scitotenv.2016.05.088.

Barnes, H., 1967, Roughness characteristics of natural channels: U.S. Geological Survey Water-Supply Paper 1849, 213 p., https://doi.org/10.3133/wsp1849.

Berenbrock, C., 2002, Estimating the magnitude of peak flows at selected recurrence intervals for streams in Idaho: U.S. Geological Survey Water-Resources Investigations Report 2002–4170, 59 p., https://doi.org/10.3133/wri20024170.

Churchill, R.K., 2000, Contributions of mercury to California's environment from mercury and gold mining activities—Insights from the historical record, *in* Extended abstracts for the U.S. Environmental Protection Agency sponsored meeting, Assessing and Managing Mercury from Historic and Current Mining Activities: San Francisco, Calif., November 28−30, 2000, Proceedings, p. 33−36 and S35−S48.

Davidian, J., 1984, Computation of water-surface profiles in open channels: Techniques of Water-Resources Investigations of the U.S. Geological Survey, Book 3, Chapter A15, https://doi.org/10.3133/twri03A15.

Fleck, J.A., Alpers, C.N., Marvin-DiPasquale, M., Hothem, R.L., Wright, S.A., Ellett, K., Beaulieu, E., Agee, J.L., Kakouros, E., Kieu, L.H., Eberl, D.D., Blum, A.E., and May, J.T., 2011, The effects of sediment and mercury mobilization in the South Yuba River and Humbug Creek confluence area, Nevada County, California: Concentrations, speciation, and environmental fate—Part 1—Field characterization: U.S. Geological Survey Open-File Report 2010–1325–A, 104 p., https://doi.org/10.3133/ofr20101325A.

Gilbert, G.K., 1917, Hydraulic-mining debris in the Sierra Nevada: U.S. Geological Survey Professional Paper 105, 154 p., https://doi.org/10.3133/pp105.

Gotvald, A.J., Barth, N.A., Veilleux, A.G., and Parrett, C., 2012, Methods for determining magnitude and frequency of floods in California, based on data through water year 2006: U.S. Geological Survey Scientific Investigations Report 2012–5113, 39 p., https://doi.org/10.3133/sir20125113.

Heritage, G.L., and Large, A.R.G., 2009, Laser scanning for the environmental sciences: Wiley-Blackwell Publishing, 288 p., http://www.wiley.com/WileyCDA/WileyTitle/productCd-1405157178.html.

Hornberger, M.I., Luoma, S.N., van Geen, A., Fuller, C., and Anima, R., 1999, Historical trends of metals in the sediments of San Francisco Bay, California: Marine Chemistry, v. 64, nos. 1–2, p. 39–55, https://doi.org/10.1016/S0304-4203(98)80083-2.

Howle, J.F., 2019, Terrestrial laser scanning data from the confluence of the South Yuba River and Humbug Creek, Nevada County, California, 2011–2013: U.S. Geological Survey data release, https://doi.org/10.5066/P9EOI74U.

Howle, J.F., Alpers, C.N., Bawden, G.W., and Bond, S., 2016, Quantifying the eroded volume of mercury-contaminated sediment using terrestrial laser scanning at Stocking Flat, Deer Creek, Nevada County, California, 2010–13: U.S. Geological Survey Scientific Investigations Report 2015–5179, 23 p., https://doi.org/10.3133/sir20155179.

Hunerlach, M.P., Rytuba, J.J., and Alpers, C.N., 1999, Mercury contamination from hydraulic placer-gold mining in the Dutch Flat mining district, California, *in* Morganwalp, D.W., and Buxton, H.T. (eds.), U.S. Geological Survey Toxic Substances Hydrology Program, Proceedings of the Technical Meeting, Charleston, South Carolina, March 8–12, 1999: U.S. Geological Survey Water-Resources Investigations Report 99–4018–B, p. 179–189, https://doi.org/10.3133/wri994018B.

Hunerlach, M.P., Alpers, C.N., Marvin-DiPasquale, M., Taylor, H.E., and De Wild, J.F., 2004, Geochemistry of mercury and other trace elements in fluvial tailings upstream of Daguerre Point Dam, Yuba River, California, August 2001: U.S. Geological Survey Scientific Investigations Report 2004–5165, 66 p., https://doi.org/10.3133/sir20045165.

James, L.A., 1989, Sustained storage and transport of hydraulic gold mining sediment in the Bear River, California: Annals of the Association of American Geographers, v. 79, no. 4, p. 570–592, https://doi.org/10.1111/j.1467-8306.1989.tb00277.x.

Kellogg, L.H., Bawden, G.W., Bernardin, T., Billen, M., Cowgill, E., Hamann, B., Jadamec, M., Kreylos, O., Staadt, O., and Sumner, D., 2008, Interactive visualization to advance earthquake simulation: Pure and Applied Geophysics, v. 165, no. 3–4, p. 621–633, https://doi.org/10.1007/s00024-008-0317-9.

Kreylos, O., Bawden, G.W., and Kellogg, L.H., 2008, Immersive visualization and analysis of LiDAR data, *in* Bebis, G., and others (eds.), Advances in visual computing: Berlin, Springer, International Symposium of Visual Computing, 2008, Lecture notes in computer science, v. 5358, p. 846–855, https://doi.org/10.1007/978-3-540-89639-5_81.

Lamontagne, J.R., Stedinger, J.R., Berenbrock, C., Veilleux, A.G., Ferris, J.C., and Knifong, D.L., 2012, Development of regional skews for selected flood durations for the Central Valley Region, California, based on data through water year 2008: U.S. Geological Survey Scientific Investigations Report 2012–5130, 60 p., https://doi.org/10.3133/sir20125130.

Marvin-DiPasquale, M., Agee, J.L., Kakouros, E., Kieu, L.H., Fleck, J.A., and Alpers, C.N., 2011, The effects of sediment and mercury mobilization in the South Yuba River and Humbug Creek confluence area, Nevada County, California: Concentrations, speciation and environmental fate—Part 2—Laboratory experiments: U.S. Geological Survey Open-File Report 2010–1325B, 53 p., https://doi.org/10.3133/ofr20101325B.

May, J.T., Hothem, R.L., Alpers, C.N., and Law, M.A., 2000, Mercury bioaccumulation in fish in a region affected by historic gold mining: The South Yuba River, Deer Creek, and Bear River watersheds, California, 1999: U.S. Geological Survey Open-File Report 2000–367, 30 p., https://doi.org/10.3133/ofr00367.

Nakamura, T.K., Singer, M.B., and Gabet, E.J., 2018, Remains of the 19th Century: Deep storage of contaminated hydraulic mining sediment along the Lower Yuba River, California: Elementa: Science of the Anthropocene, v. 6, article 70, 17 p., https://doi.org/10.1525/elementa.333.

Stumpner, E.B., Alpers, C.N., Marvin-DiPasquale, M., Agee, J.L., Kakouros, E., Arias, M.R., Kieu, L.H., Roth, D.A., Slotton, D.G., and Fleck, J.A., 2018, Geochemical data for water, streambed sediment, and fish tissue from the Sierra Nevada Mercury Impairment Project, 2011–12: U.S. Geological Survey Data Series 1056, 133 p., https://doi.org/10.3133/ds1056.

U.S. Army Corps of Engineers, 2010, HEC-RAS River Analysis System, version 4.1 User's Manual: Davis, Calif., U.S. Army Corps of Engineers, Hydrologic Engineering Center [variously paged], http://www.hec.usace.army.mil/software/hec-ras/documentation.aspx.

Veilleux, A.G., Cohn, T.A., Flynn, K.M., Mason, R.R., Jr., and Hummel, P.R., 2014, Estimating magnitude and frequency of floods using the PeakFQ 7.0 program: U.S. Geological Survey Fact Sheet 2013–3108, 2 p., https://doi.org/10.3133/fs20133108.

Wentworth, C.K., 1922, A scale of grade and class terms for clastic sediments: Journal of Geology, v. 30, no. 5, p. 377–392, https://doi.org/10.1086/622910.

Glossary

Angle of repose The maximum angle, relative to the horizontal plane, at which sediment of a given particle size and degree of rounding remains stable, without sliding down slope.

Colluvial slope A general term for loose, unconsolidated sediments that have been eroded from a higher slope position (typically a steeper slope) and deposited down slope (typically on a lower angle slope) by gravity-driven processes.

Debris flow A general term for a fast-moving mass of water-saturated sediment (of varying size) that typically originates from a steep slope during high-intensity rain events and eventually comes to rest on a lower-angled slope when the sediment is no longer saturated with water.

Dry ravel A general term that describes the gravity-driven rolling, bouncing, and sliding of sediment particles down a slope.

Hardrock mining A type of mining where a tunnel, shaft, or open pit is dug, blasted, or drilled out of solid rock for the purpose of extracting minerals or metal-bearing rock, referred to as ore.

Hydraulic gold mining A type of surface mining where a high-pressure jet of water (emitted from a water cannon, or monitor) is used to dislodge or erode gold-bearing sedimentary deposits that are exposed on a hillside or cliff face.

Lidar Light detection and ranging, which is a remote-sensing technology used to make precise three-dimensional point clouds of the land surface. Pulses of near-infrared laser light are timed to measure the distance (range) from the laser scanner to the reflecting surface. Laser ranges are combined with angular orientation data to generate a dense and detailed set of points (locations of individual laser returns), referred to as a point cloud.

Mining debris Waste materials from mining and mineral processing including waste rock, mill tailings, and alluvium from hydraulic mining.

Placer mining Mining of an unconsolidated alluvial or colluvial deposit (placer deposit). Typically, placer deposits are mined by surface methods (hydraulic mining or dredging); in some cases underground methods (drift mining) are used. Metallic clasts and mineral grains are gravity separated by means of hydraulic saturation and mechanical agitation.

Point cloud A point cloud is a set of vertices in a three-dimensional coordinate system. These vertices are usually defined by x, y, and z coordinates and typically represent the external surface of an object.

Terrestrial laser scanning (TLS) Sometimes referred to as ground-based lidar or terrestrial lidar (T-lidar). The significance of ‘terrestrial’ refers to the laser scanner being near the Earth’s surface (stationary on a tripod) as opposed to airborne laser scanning.

Appendix 1.

Table 1–1. Measured sediment mass and volume from vertical traverses of the cliff, over-steepened slope, and colluvial slope areas; calculated density; average density for various areas; and relative uncertainty of density in percent.

[g, gram; g/cm^3, grams per cubic centimeter;—, not applicable; %, percent]

Area	Sample number	Vertical traverse	Mass (g)	Volume (cm^3)	Density (g/cm^3)	Average density (g/cm^3)	Relative standard deviation
Cliff	CL-1	East	713	390	1.83	—	—
Cliff	CL-2	East	833	390	2.14	—	—
Cliff	CL-3	Middle	729	405	1.80	—	—
Cliff	CL-4	Middle	824	405	2.03	—	—
Cliff	CL-5	West	802	411	1.95	—	—
Cliff	CL-6	West	896	402	2.23	—	—
Cliff	—	—	—	—	—	2.00	8%
Over-steepened slope	OS-1	East	699	405	1.73	—	—
Over-steepened slope	OS-2	East	709	405	1.75	—	—
Over-steepened slope	OS-3	Middle	718	390	1.84	—	—
Over-steepened slope	OS-4	Middle	707	399	1.77	—	—
Over-steepened slope	OS-5	West	739	405	1.82	—	—
Over-steepened slope	OS-6	West	731	405	1.80	—	—
Over-steepened slope	—	—	—	—	—	1.79	2%
Colluvial slope	[1]CS-2	East	606	377	1.61	—	—
Colluvial slope	CS-3	Middle	671	411	1.63	—	—
Colluvial slope	CS-4	Middle	607	411	1.48	—	—
Colluvial slope	CS-5	West	691	411	1.68	—	—
Colluvial slope	CS-6	West	636	399	1.59	—	—
Colluvial slope	—	—	—	—	—	1.60	5%
Average density of cliff and over-steepened slope samples (n=12)						1.89	9%

[1]Sample CS-1 was omitted from the colluvial slope density analysis because of a procedural difference in collecting the sample relative to the other colluvial slope samples.

For more information concerning the research in this report, contact the
Director, California Water Science Center
U.S. Geological Survey
6000 J Street, Placer Hall
Sacramento, California 95819
https://ca.water.usgs.gov

Publishing support provided by the U.S. Geological Survey
Science Publishing Network, Sacramento Publishing Service Center

ISSN 2328-0328 (online)
https://doi.org/10.3133/sir20195104